Engineered Regeneration 6 (2025) 1–16

Contents lists available at ScienceDirect

Engineered Regeneration

journal homepage: http://www.keaipublishing.com/en/journals/engineered-regeneration/

Integrating bioprinted oral epithelium with millifluidics for fluorouracil perfusion and Fusobacterium infection to bioengineer oral mucositis-on-a-chip

Tien T.T. Truong[a,b,1], Toan V. Phan[a,b,1], Yamin Oo[a], Ladawan Sariya[c], Risa Chaisuparat[a,d], Silvia Scaglione[e,f], Glauco R. Souza[g,h], Supansa Yodmuang[a,i], Catherine H.L. Hong[j], Kai Soo Tan[j], Waranyoo Phoolcharoen[k], Oranart Matangkasombut[l,m], João N. Ferreira[a,*]

[a] Center of Excellence and Innovation for Oral Health and Healthy Longevity, Faculty of Dentistry, Chulalongkorn University, Bangkok, 10330, Thailand
[b] International Graduate Program in Oral Biology, Faculty of Dentistry, Chulalongkorn University, Bangkok, 10330, Thailand
[c] The Monitoring and Surveillance Center for Zoonotic Diseases in Wildlife and Exotic Animals, Faculty of Veterinary Science, Mahidol University, Nakhon Pathom, 73170, Thailand
[d] Department of Oral Pathology, Faculty of Dentistry, Chulalongkorn University, Bangkok, 10330, Thailand
[e] Institute of Electronic, Computer and Telecommunications Engineering (IEIIT), National Research Council of Italy, Genova, 16149, Italy
[f] React4life S.p.A., Genova, 16152, Italy
[g] ChemoSen3D, Houston, TX, 77054, USA
[h] Global Business Development and Innovation, Greiner Bio-one N.A., Charlotte, NC, 28110, USA
[i] Department of Research Affairs, Faculty of Medicine, Chulalongkorn University, Bangkok, 10330, Thailand
[j] Faculty of Dentistry, National University of Singapore, 119085, Singapore, Singapore
[k] Department of Pharmacognosy and Pharmaceutical Botany, Faculty of Pharmaceutical Sciences, Chulalongkorn University, Bangkok, 10330, Thailand
[l] Department of Microbiology and Center of Excellence on Oral Microbiology and Immunology, Faculty of Dentistry, Chulalongkorn University, Bangkok, 10330, Thailand
[m] Research Laboratory of Biotechnology, Chulabhorn Research Institute, Bangkok, 10210, Thailand

ARTICLE INFO

Keywords:
Chemotherapy
Epidermal growth factor
Oral keratinocytes
Nicotiana benthamiana
Plant molecular farming
Millifluidics

ABSTRACT

Oral mucositis (OM) remains a painful complication of anticancer chemotherapy (CT), tending to progress in severity in the presence of *Fusobacterium nucleatum* (*Fn*). Yet, no effective therapy exists to suppress OM since *in vitro* models mimicking CT-induced OM are lacking, halting the discovery of new drugs. Here, we developed an integrated millifluidic *in vitro* tissue culture system for OM disease modeling. This bioengineered system integrates magnetically bioassembled oral epithelium sheets with millifluidics for CT-based 5-fluorouracil perfusion and *Fn* infection to model CT-induced OM. After modeling OM with all pro-inflammatory hallmarks, we were able to suppress OM with our in-house plant-produced epidermal growth factor (P-EGF), a well-known re-epithelialization cue. Thus, this the first instance where a millifluidic system enabled OM modeling in the presence of CT drug perfusion and *Fn* infection. This bioengineered system is a novel tool for drug discovery as it propelled P-EGF as a promising therapy for OM.

1. Introduction

Oral mucositis (OM) is one of the most debilitating oral complications of cancer treatment, including chemotherapy (CT), and a manifestation observed in up to 100 % head and neck cancer patients [1,2]. Those OM lesions frequently progress to painful oral ulcerations, which adversely affect patient's diet and proper nutrition, thus negatively impacting their quality of life.

The role of the oral microbiome in OM pathogenesis is just beginning to be unveiled. Our group demonstrated that the oral flora has a detrimental effect on CT-induced OM in vivo, whereas the oral mucosa of 5-fluorouracil (5FU)-treated germ-free mice presented higher epithelial cell proliferation, lower levels of pro-inflammatory cytokines and increased oral epithelial thickness when compared to 5FU-treated specific pathogen free mice [3]. Elsewhere, researchers have reported on the impact of the oral microbiome in the progression of OM during can-

* Corresponding author at: 34 Henri-Dunant Rd, Pathumwan, 10330, Bangkok, Thailand.
E-mail address: Joao.F@chula.ac.th (J.N. Ferreira).
[1] These authors contributed equally.

https://doi.org/10.1016/j.engreg.2025.02.001
Received 21 November 2024; Received in revised form 6 February 2025; Accepted 12 February 2025
Available online 14 February 2025

cer therapy [4,5]. The abundance of the anaerobic *Fusobacterium* genus was consistently reported to coincide with the peak of severe OM after CT, especially the species *Fusobacterium nucleatum (Fn)* [6]. Despite being a predominant species in the oral cavity of healthy subjects, the high abundance of *Fn* during cancer treatment is thought to be related with the OM onset. *Fn* subspecies or clades are not usually found in the gut microbiome of healthy individuals; yet, specific clades are highly enriched in human colorectal cancer tissues, and these *Fn* clades seem to predict cancer progression [7].

Currently, there is no effective management strategy for OM [8]. Symptom-based care remain the cornerstone of this adverse complication. However, mucosal healing requires re-epithelialization which comprises both epithelial cell proliferation and migration [9]. Presently, the only approved drug to ameliorate OM via re-epithelialization is palifermin or keratinocyte growth factor, which was completely or temporarily withdrawn from the market recently in several countries due to systemic and cancer-related complications [10]. Hence, these recent developments directed researchers to explore alternative cues such as epidermal growth factor (EGF), which shares a similar conceptual role with palifermin for enhancing oral epithelial repair [11].

Noteworthy biological effects of EGF in a murine OM model have been observed including a robust improvement of epithelial proliferation and thickness, indicating beneficial outcomes in preclinical trials [12], as well as in randomized clinical trials [13]. Commercially available recombinant human EGF, produced using *Escherichia coli*-based conventional biotechnology platforms, offers advantages such as cost-effectiveness, rapid production, and scalability [14]. Nevertheless, this bacterial production platform presents challenges including the lack of post-translational modifications, protein aggregation, misfolding, and potential contamination with endotoxins, prompting a research interest in plant molecular farming as a viable alternative. Plant production systems offer several benefits including reduced pathogen contamination risk, lower production costs, high scalability, and the capability for post-translational modifications. *Nicotiana benthamiana*, known for its rapid growth (3-4 weeks) and ease of genetic manipulation, is frequently used for recombinant protein production [15]. Our research team has successfully used *N. benthamiana* to produce EGF (plant-produced EGF or P-EGF), which showed promising results in enhancing the proliferation and migration of skin and oral epithelial keratinocytes [16,17]. Moreover, our research team can also produce epithelial three-dimensional (3D) functional models (a.k.a. organoids) by tagging primary cells with a novel solution of magnetic nanoparticles (Nanoshuttle^{TM}) - composed of iron oxide, gold, and poly-L-lysine – to then assemble them in 3D tissues via magnetic bioassembly or bioprinting [18].

Despite these research endeavors and due to lack of OM models in millifluidic systems resembling the physiological niche as in vivo, the effectiveness of P-EGF in reversing the cytotoxicity of 5FU chemotherapeutic agent remains unknown, particularly in the context of oral epithelial interfaces in the presence of OM-associated anaerobes such as *Fn*. This research gap underscores the importance of bioengineering strategies to develop in vitro disease models with 5FU-based fluid flow from 3D oral epithelial sheets (OES). Tackling these CT-driven oral diseases, millifluidic microphysiological systems (MPS) developed by our researchers at React4Life company [19,20] were used for exploring the homeostasis and disease mechanisms in the interface between oral epithelia and OM-associated bacteria. These OM 5FU-based millifluidic models are currently needed despite a few efforts of other research groups using static organotypic models [21,22] and microfluidic platforms with cisplatin exposure [23,24]. The critical intravenous body fluid dynamics in CT can only be properly emulated with millifluidic systems due to poorly controlled resistance and high shear stress within the narrow channels and chambers used in microfluidics [25,26]. Hence, this study aims to: (1) bioengineer and validate 5FU-based fluidic OM models in the presence of *Fn* stimuli; and (2) to interrogate whether P-EGF can effectively ameliorate OM inflammatory hallmarks and promote epithelial repair in the presence of *Fn* stimuli. Briefly, OES constructs are bioprinted using magnetic bioassembly platforms after pre-tagging human oral keratinocytes with Nanoshuttle. Next, these are transferred to a microphysiological system using a millifluidic set up at optimized laminar flow speeds. Those dynamic flow settings were used for chemotherapeutic drug 5FU perfusion and the delivery of P-EGF, towards interrogating OM disease mechanisms and potential therapeutic roles, respectively.

2. Materials and methods

2.1. Cell culture and OES biofabrication

Human normal oral keratinocytes (NOKs) were provided and authenticated by Prof. Chidchanok Leethanakul (Prince of Songkhla University) according to a previously published protocol [27]. These cells were tested on a regular basis for mycoplasma contamination using DNA staining and PCR methods. NOKs were cultured in defined keratinocyte growth media (DKSFM, Gibco, Thermo Fisher Scientific, MA, USA) mixed with Dulbecco's Modified Eagle Medium F12 (DMEM/F12, Sigma Aldrich, Merck, Germany) at ratio of 1:1, and the media was changed every two days.

For the generation of oral epithelial sheets (OES), NOKs reaching to 80–90 % confluence were tagged with magnetic nanoparticles (MNP) solution with the tradename Nanoshuttle (Greiner Bio-One, Frickenhausen, Germany) at concentration of 1 μl per 1.5×10^5 cells overnight. On the next day, MNP-tagged cells were dissociated and seeded in DFK media with 2 mM $CaCl_2$ at density of 2×10^5 cells/well in a 24-well plate precoated with 150 μl agarose (Sigma-Aldrich). A magnetic drive was placed at the bottom of the plate for 2 days to facilitate the bioassembly and bioprinting of the OES tissue constructs. Following removal of the magnetic drive, assembled cell sheets were maintained in culture for an additional 2 days for self-organization, and the media was changed every 2 days. OES were analyzed for their morphology using a high-resolution flatbed scanner for image acquisition, the Epson Perfection V600 Flatbed Scanner (Seiko Epson Corporation, Suwa, Nagano, Japan), and ImageJ software (version 1.54 g, Bethesda, MD, NIH) was utilized to measure all morphological features.

After the magnetic bioassembly of the OES tissue constructs, these were placed inside a dynamic and nearly microphysiological microenvironment within the MIVO® millifluidic platform (React4life, Italy), whereas each sheet was transferred to a transwell insert (Greiner Bio-one, Germany) inside a donor chamber. This insert was subsequently placed in the receiving chamber, connected to a peristaltic pump device at an optimal flow rate of 10 mm/s with 3 mL of maximum medium volume (Fig. 1A and 3A). This velocity was chosen based on our preliminary experiments where this was adjusted to optimize epithelial cell viability. OES were maintained in the system for another two days.

2.2. Modeling CT-induced OM via 5FU media supplementation

After 4 days of OES bioprinting, 5-Fluorouracil (5FU) (Sigma-Aldrich) with concentration of 0, 50, 500 μg/ml was added for 24 h. To evaluate the effect of *Nicotiana benthamiana* plant-produced EGF (P-EGF) in rescuing cell sheet viability after 5FU cytotoxic exposure, media with 5FU was replaced with media containing varying concentration of P-EGF (0, 50, 100, 200 ng/ml) and sheets were cultured for another 24 h.

2.3. Modeling Fn exposure in CT-induced OM models

Fusobacterium nucleatum (ATCC 25586, ATCC) (*Fn*) were cultured in Tryptone Soya Agar (Himedia, MUM, India) supplemented with 5 % human blood in an anaerobic jar. The colonies were transferred to brain heart infusion broth (Himedia) supplemented with vitamin K (1 μg/ml) and hemin (5 μg/ml). *Fn* in log phase (OD_{600}=0.6-0.8) was collected by centrifugation at 6000 x g for 10 min at 4 ˚C. Bacterial pellets were

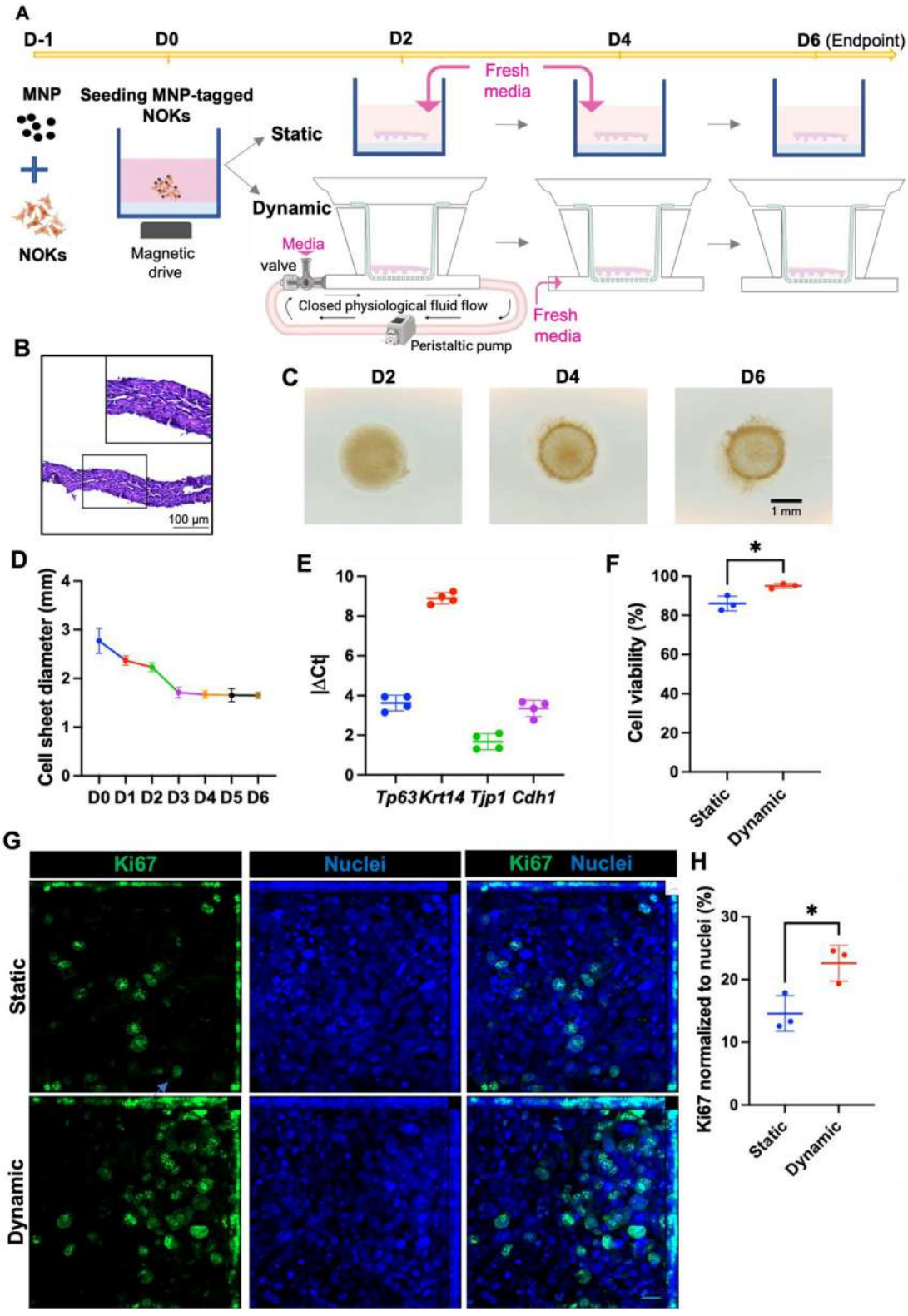

Fig. 1. Biofabrication of 3D oral epithelial sheet (OES) and its proliferation and pro-mitotic features in static and dynamic millifluidic systems. (A) Workflow for generating the OES in static and dynamic conditions. Figure created with BioRender.com (**B**) H&E staining of the bioprinted OES. (**C**) OES morphology as per imaging acquired with a high-resolution flatbed scanner and (**D**) displays the OES diameter through time quantified with ImageJ software, n = 4. (**E**) Epithelial gene expression was detected using qPCR and plotted as $|\Delta CT|$ where $\Delta CT = CT_{\text{gene of interest}} - CT_{Rps29}$, where *Rps29* represents the house keeping gene, and n=4/group. (**F**) Cell sheet viability between static and dynamic conditions determined by Trypan Blue exclusion assay. Data are displayed as mean ± SD and a two-tailed Student's *t*-test was performed, n = 3: $^{*}p < 0.05$. (**G, H**) Expression of proliferation marker Ki67 in OES and counterstaining with nuclear Hoechst. (**G**) Micrographs were acquired with confocal microscopy at 40X magnification as maximum intensity projection of a z-stack sidelined by XYZ orthogonal projections. Scale bar: 20 μm (**H**) Ki67 expression was quantified by ImageJ software and normalized to total nuclei. Data are presented as means ± SD and a two-tailed Student's *t*-test was performed, n = 3: $^{*}p < 0.05$.

washed three times and resuspended in PBS. Heat-killed *Fn* was obtained by heating at 60 ˚C for 40 min and stored at -80 ˚C prior to use. The complete killing of *Fn* was confirmed by plating. Heat-killed *Fn* was added to epithelial sheets at multiplicity of infection (MOI) of 0, 10, 50, 100 and 200. Next, cells were further incubated at 37 ˚C and 5 % CO_2 for 24 h. The lowest MOI that gives a significant increase in proinflammatory cytokine expression was chosen for further experiments.

2.4. Cell viability assays

Cell sheet viability was determined by Trypan blue exclusion assay. Briefly, epithelial sheets were dissociated with TrypLE select (Thermo Fisher Scientific) for 30 min. The cell suspension was pipetted up and down every 10 min. Cell pellet was collected by centrifugation at 10,000 rpm for 5 min and subsequently resuspended with 100 μl media. Cell suspension was diluted with trypan blue, and viable cells was counted using a hemacytometer.

2.5. Gene expression array and analysis

Gene expression in epithelial cell sheets was analyzed using quantitative polymerase chain reaction (qPCR). Total RNA was extracted using the Monarch® Total RNA Miniprep Kit (New England Biolabs) and converted to cDNA with SuperScriptTM III (ThermoFisher Scientific). SYBR® Green-based qPCR was performed using primers listed in Table S1, employing the QuantStudio 3 Real-Time PCR System (ThermoFisher Scientific). The relative expression of target genes was quantified using the ΔCT or $2^{-(\Delta\Delta CT)}$ method, normalized against the housekeeping gene *Rps29* and compared to untreated control groups. All oligonucleotide primers were listed in Supplementary Table S1.

2.6. Immunofluorescence and immunohistochemistry

Antibodies listed in Supplementary Table 1 were used to phenotypically characterize epithelial sheets and access the responses of cell sheets to 5FU and P-EGF treatment by immunofluorescence. Sheets were fixed with 4 % paraformaldehyde for 10 min. After fixation, Triton-X 0.1 % was added for permeabilization, and sheets were subsequently washed three times with 1x PBS before a 2-hour incubation with blocking buffer. Primary antibodies were incubated overnight at 4 ˚C, followed by a PBS wash step and the addition of the anti-rabbit secondary antibodies labeled with AlexaFluor 488 or with AlexaFluor 594 (ab150077 and ab150080; Abcam). Finally, Hoechst 33342 (Thermo Fisher Scientific) was added and incubated for 20 min. Confocal microscope (Zeiss LSM 980, Germany) was used to visualize the staining, and the percentage of cells expressing these markers was quantified using Fiji/ImageJ version 1.54 g, except for $\gamma H2AX$ assessment where all nuclei were detected by the “analyze particles” function and all the foci in each nucleus were counted. All data was normalized to cell density.

2.7. Western blot

For the Western blot assays, proteins from 2D, static, and dynamic culture were extracted from cell lysates using a RIPA buffer supplemented with protease inhibitors (Thermo Fisher Scientific). Protein concentrations were determined by the BCA assay (Thermo Fisher Scientific). Equal amounts of protein (20–40 μg) were separated by SDS-PAGE on a 10 % polyacrylamide gel (Merck) and subsequently transferred onto PVDF membranes. The membranes were blocked with 5 % non-fat dry milk in TBST (Tris-buffered saline with 0.1 % Tween-20) for 1 h at room temperature. Following blocking, the membranes were incubated overnight at 4°C with primary antibodies including K14 (ab181595; Abcam), PCNA (ab18197; Abcam), GAPDH (sc365062; Santa Cruz). After washing three times with TBST, the membranes were incubated with HRP-conjugated secondary antibodies (diluted 1:5000 in TBST) for 1 h at room temperature. Detection was performed using a Western Blotting Luminol Reagent (Santa Cruz), and the signal was captured using ChemiDoc (Biorad). Band intensities were quantified using ImageLab software version 3.0.3, and protein levels were normalized to GAPDH as an internal control.

2.8. Migration assays

Epithelial sheets in millifluidic system were used to test for their migration capabilities. Following two-day bioprinting, sheets were transferred to inserts with 8-μm pores and maintained for a further 2 days of culture. On the day fourth, 5FU was introduced to the fluid flow in receiver chamber for a duration of 24 h. Following this treatment, receiver chamber was replenished with fresh media, and heat-killed *Fn* (HKFn) along with P-EGF were added on top of sheets in donor chamber for an additional 24 h. Migration of cells was assessed by staining with Hoechst 33341 and observed under EVOS FL Auto II fluorescence microscope (Thermo Fisher Scientific).

2.9. Enzyme-linked immunosorbent assay

The level of IL-6 and IL-8 in the supernatant is quantified by ELISA MAX^{TM} Deluxe Set Human IL-6 (Biolegend, SD, USA) and ELISA MAX^{TM} Deluxe Set Human IL-8 (Biolegend) following the instruction of the manufacturer. To analyze IL-6 and IL-8 in cell sheet, cell lysate was achieved using RIPA buffer (Thermo Fisher Scientific) mixed with 1X protease inhibitor cocktail (Himedia) according to manufacturer’s instruction.

2.10. Intracellular calcium influx assay

To evaluate the intracellular calcium ion mobilization on OES tissue constructs in the OM model after injury was inflicted via scrapping within the dynamic millifluidic system, the cell sheets in the donor chamber, after a 24 h 5FU treatment and a subsequent 24 h period with heat-killed Fn and P-EGF addition, were transferred to a 24-well plate. The calcium-labelled reagent 2x Fluo-4 Direct (Thermo Fisher Scientific) was diluted to 1x with an equal volume of culture media. After 1 h incubation, a controlled hole was introduced to each sheet using a pipette tip (1/32 inches), and calcium influx in cell sheets were monitored real-time in the onstage incubator under time-lapsed fluorescence microscopy.

2.11. Statistical analysis

Statistical analysis was performed with GraphPad Prism version 9.5.3 (GraphPad, San Diego, CA, US). Data resulting from each experimental assay were tested for normality with Shapiro-Wilk test and for equal variance assumptions (Welch’s t-test) before the use of parametric statistical testing. In the case where either of those assumptions was infringed, the corresponding datasets were nonlinearly transformed to satisfy those assumptions. Data were collected and plotted as mean ± standard deviation (SD) from biological replicates. Each biological replicate data point represents the average of technical replicates for that experiment. Differences between two groups were evaluated by a two-tailed unpaired *Student’s t*-test. One-way ANOVA analysis followed by post-*Tukey’s* multiple comparison tests were used to compare more than two groups (details of ANOVA tests are indicated in the captions of each figure). Statistical significance of the data was calculated at the 95 % confidence interval.

3. Results

3.1. Oral epithelial cell sheet biofabrication and characterization in static and dynamic millifluidic systems

Epithelial cell sheets were established from normal oral keratinocytes (NOKs) using magnetic three-dimensional bioprinting

(M3DB) as a first step in the biofabrication process. (Fig. 1A). After two days of culture, NOKs clustered and developed into a sheet-like tissue construct with a multilayered architecture, reaching a thickness of 80 ± 5 μm (Fig. 1B). This morphology was maintained until day 6 of culture (Fig. 1C) and the sheet diameter reached a plateau from day 3 to day 6 (Fig. 1D). Cell sheets formed from NOKs expressed basal oral epithelial cell markers such as *Tp63, Krt14, Cdh1* (Fig. 1E). Epithelial differentiation and stratification were also observed as per the expression of *Tjp1* and *zonula occludens*-1 (ZO-1) and involucrin in specific outer layers (Fig. 1E, Fig. S1). To better resemble in part the physiological nutrient/metabolic flow in vivo, epithelial cell sheets were placed inside a transwell insert within a millifluidic dynamic chamber (MIVO®), and media fluid flow in the bottom of the transwell was possible by using a peristaltic pump device (Fig. 1A). The application of this millifluidic system simulating a dynamic laminar flow microenvironment led to a significant increase in cell sheet viability when compared to static culture conditions (Fig. 1F).

Immunohistochemistry revealed a marked upregulation of Ki67 cell proliferation marker within the dynamically cultured cell sheets (Fig. 1G, H). This was later confirmed with western blot assay assessing the expression of proliferating cell nuclear antigen (PCNA) (Fig. 2A, B). Protein expression levels of cytokeratin 14 (K14), a marker for basal keratinocytes, remained unchanged across both culture conditions (Fig. 2A, C, F, G). To access oral epithelial integrity and tissue barrier function of the bioprinted sheet, transepithelial electrical resistance (TEER) was measured, and higher TEER values were found with the dynamic millifluidic integrated system compared to the static one. To confirm these findings at the intercellular level, cell-cell epithelial connectivity and compaction across the stratified epithelia were evaluated using immunostaining for E-cadherin (Ecad) and desmoglein-3 (Dsg3). The dynamic system strikingly promoted the expression of Ecad and Dsg3, indicating an enhanced formation of cell *adherens* and adhesive epithelial junctions (Fig. 2F, H, I). Expression of ZO-1 was also observed (Fig. S1). Collectively, these findings suggested that both static and dynamic millifluidic integrated systems can support and maintain a bioprinted 3D OES model. Furthermore, the dynamic platform appeared to robustly improve the overall viability and epithelial tissue barrier properties and function of the bioprinted OES interface.

3.2. *5FU and* Fusobacterium nucleatum *induced cytotoxicity and pro-inflammatory cytokine secretion in bioprinted OES tissue constructs*

To develop an OM model in an integrated millifluidic system (MIVO®) for investigating CT-induced damage in the oral epithelia interface, different concentrations of 5FU were perfused in the bioprinted OES tissue constructs (Fig. 3A). A significant reduction in cell viability was observed beginning at a 5FU dose of 5 µg/ml; while 500 µg/ml of 5FU resulted in a substantial decrease in epithelial viability. Thus, this 5FU dose was selected for further experiments to establish a more robust and predictable OM model (Fig. 3B). The biological effects of *Fn* on OES were assessed by exposure to *F. nucleatum* at multiplicities of infection (MOI) of 10, 50, 100, and 200. Viability assays revealed no major changes in the cell sheet viability across these conditions (Fig. 3C). However, a dose-dependent increase in the secretion of pro-inflammatory cytokines IL-6 and IL-8 was observed, suggesting an inflammatory response to *Fn* (Fig. 3D, E). Although no significant differences in cytokine release were observed between MOI 50 and 100, MOI 100 was selected to provide a more stringent condition for evaluating the effectiveness of P-EGF. The outcomes obtained at MOI 100 produced fewer biological variations as compared to MOI 50 (Fig. 3D-E), safeguarding the reproducibility of the experiments and consistency of the data. A MOI of 100 was selected to further evaluate the cytokine response profile. When 5FU-induced OM-like OES were exposed to *Fn*, there was an additional 10 % reduction in viability (Fig. 3F) and a marked increase in IL-6 and IL-8 expressions compared to OM-like OES treated with 5FU alone (Fig. 3G-H). This underscores the heightened vulnerability of the OM model to bacterial challenges post-CT in the millifluidic system.

3.3. *Rescuing effects of P-EGF on OM integrated model after* Fn *exposure*

P-EGF treatment delivered in the OM interface model (post-5FU exposure) via media supplementation led to a dose-dependent increase in OES viability in the context of the millifluidic system. Specifically, P-EGF at 100 ng/ml significantly enhanced cell viability, with no notable differences observed upon a dosage increase to 200 ng/ml of P-EGF (Fig. 4A). This suggested an optimal therapeutic window for P-EGF in promoting OES cell survival in the OM-like condition (5FU-treated). In OM-like OES exposed to *Fn*-containing media, P-EGF only demonstrated a minor protective effect, improving cell viability by 5 % (Fig. 4B). Gene expression of epithelial markers *Tp63, Tjp1, Cdh1* decreased significantly with 5FU (OM-like system), and P-EGF treatment did not change the expression of these genes (Fig. 4C, E, G-J). In contrast, *Krt14* expression was elevated after 5FU exposure, and further increased with P-EGF treatment only when *Fn* was present (Fig. 4D, F). Moreover, P-EGF triggered changes in E-cadherin (Ecad) protein expression. In the OM group, the expression of Ecad was less pronounced, and the intercellular distribution of the cell-cell adhesion protein appeared more fainted circling rounded-shape cells. This damage was more marked in OM exposed to *Fn* (Fig. 4K). Yet, upon P-EGF treatment the polygonal shape of epithelial cells in OM-like OES was restored and Ecad distribution was more robust in both with and without *Fn* stimuli.

Furthermore, DNA damage was evaluated via the accumulation of $\gamma H2AX$, a sensitive specific molecular marker for monitoring the repair DNA double-strand breaks (DSBs) (Fig. 5). OM (5FU-treated only) upregulated the H2ax mRNA expression compared to control (CTL) OES, but not in statistical terms (Fig. 5A). P-EGF treatment resulted in a relevant increase in the expression of *H2ax*, significantly higher than those observed in both control OES (Fig. 5A) and the OM OES system exposed to 5FU only (Fig. 5B). However, H2ax mRNA is not a direct marker to assess the repair of DNA DSBs. The specific indicator of DNA DSBs repair is the $\gamma H2AX$ protein. The level of $\gamma H2AX$ was increased in OM OES (post-5FU) and this was suppressed upon P-EGF administration (Fig. 5C-E), indicating that such DNA repair was resolved with P-EGF. The level of $\gamma H2AX$ was as high in OM OES models exposed to *Fn* compared to no *Fn* (Fig. 5C-E), and P-EGF administration was able to decrease the expression of this marker but not at the same level as when *Fn* stimuli was absent (Fig. 5C-E).

These findings suggest that P-EGF in the presence of *Fn* can restore the viability of the OES in the OM-like integrated interface model, promote the formation of intercellular epithelial cell adhesion communications, normal epithelial compaction and morphology, leading to the resolution of DNA damage.

3.4. *Inflammatory cytokine release and epithelial migration in OM millifluidic model after P-EGF administration*

To examine whether P-EGF administration enhances epithelial response to oxidative stress induced by 5FU in the OM model in the presence of *Fn*, the expression and nuclear translocation of the nuclear factor E2-related factor 2 (Nrf2) was determined using immunohistochemistry and confocal microscopy (Fig. 5F). In the OM OES model, there was an overall increase in Nrf2 expression compared to the OES control (not mimicking OM). Treatment with P-EGF resulted in greater nuclear translocation of Nrf2 compared to the untreated OM model (OM OES). Following the exposure to *Fn* in the OM model (OM OES+*Fn*), Nrf2 translocation was less marked compared to the *Fn*-free OM model (OM OES), although its expression was higher relative to OES control. Still, with subsequent P-EGF administration, Nrf2 expression and nuclear translocation were again elevated (Fig. 5F).

To investigate whether P-EGF administration reduces the pro-inflammatory response found in OM models following *Fn* exposure, the

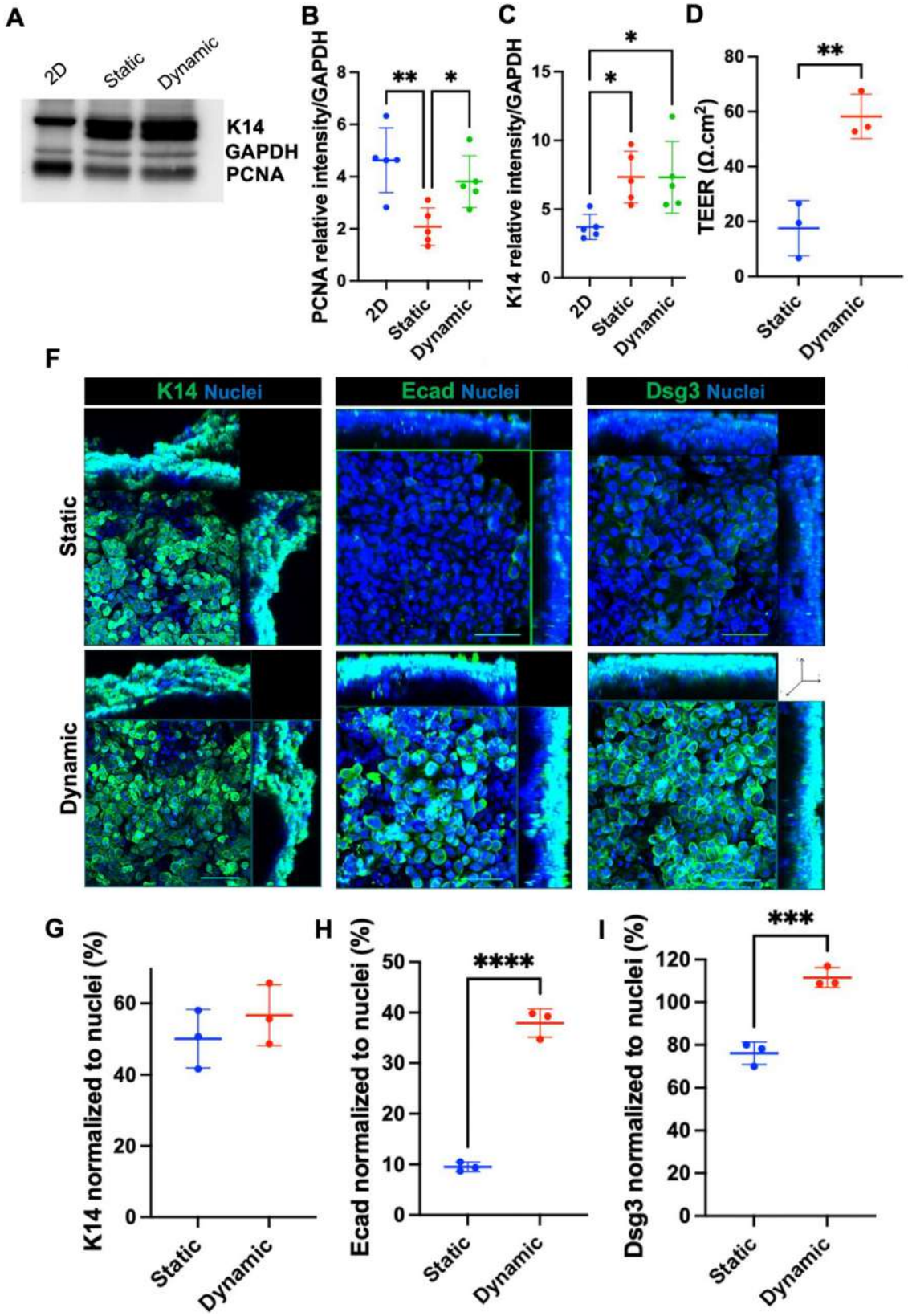

Fig. 2. Characterization of OES in static and dynamic millifluidic systems. (A-C) Expression of K14, PCNA and the house keeping marker GAPDH (loading control) in immunoblots followed by western blot analysis and protein band quantification. The uncropped full-length gel is displayed in Supplementary Fig. S3. Data are presented as mean ± SD, and one-way ANOVA with post-hoc *Tukey's* test was performed, n = 4: $^{*}p < 0.5$, $^{**}p < 0.01$. (**D**) Transepithelial electrical resistance measurements to assess oral epithelial tissue barrier function of OES. (**F**) Confocal micrographs showing immunoreactivity for K14, Ecad and Dsg3 oral epithelial markers in maximum intensity projections from z-stacks sidelined with XYZ orthogonal projections after whole mount immunohistochemistry of OES. Scale bar: 50 μm. (**G-I**) The expression of such oral epithelial markers was quantified by ImageJ software, data are normalized to total nuclei and are plotted as mean ± SD, and a two-tailed Student's *t*-test was performed: $^{***}p < 0.001$, $^{****}p < 0.0001$.

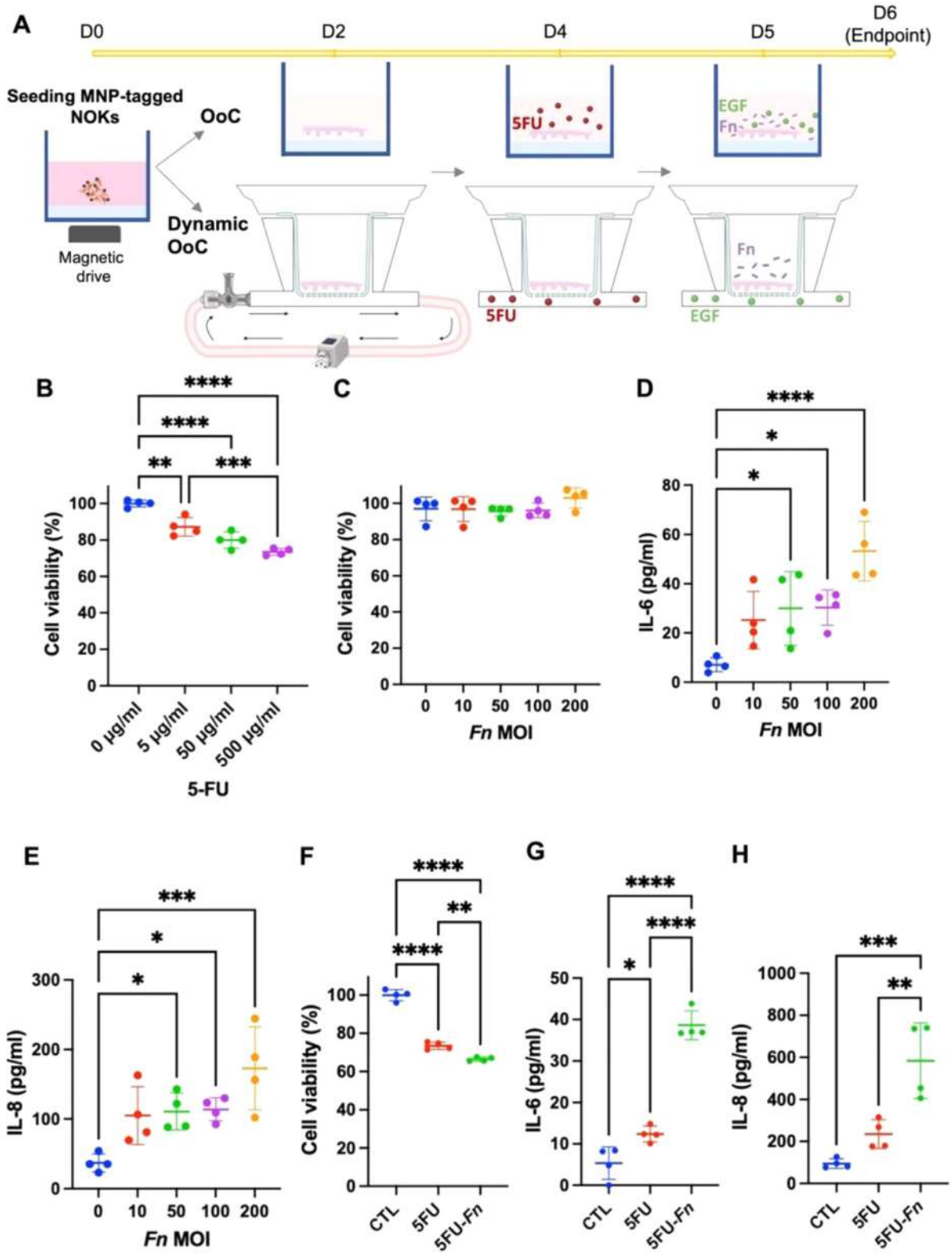

Fig. 3. OM disease modeling with *Fn* exposure of OES. (A) Bioengineering steps for OM modeling in the integrated bioprinted OES tissue constructs with the millifluidic system. Figure created with BioRender.com. (**B**) Viability of OES following 24 h of chemotherapy-like 5FU treatment determined by trypan blue. Data are plotted as mean ± SD and one-way ANOVA with post-hoc *Tukey's* test was performed, n = 4: $^{**}p < 0.01$, $^{***}p < 0.001$, $^{****}p < 0.0001$. (**C**) Viability of OES upon increasing *Fn* multiplicities of infection (MOI). Data are plotted as mean ± SD and one-way ANOVA post hoc *Tukey's* test was performed, n = 4. (**D-E**) Pro-inflammatory cytokine secretion upon increasing *Fn* MOI measure by ELISA. Data are plotted as mean ± SD and one-way ANOVA with post-hoc *Dunnet's* test was performed, n = 4: $^{*}p < 0.5$, $^{***}p < 0.001$, $^{****}p < 0.0001$. (**F**) Viability of OES. Data are plotted as mean ± SD and one-way ANOVA with post-hoc *Tukey's* test was performed, n = 4: $^{**}p < 0.01$, $^{***}p < 0.001$, $^{****}p<0.0001$. (**G-H**) Pro-inflammatory cytokine secretion by ELISA following sequential 24 h treatment with 5FU followed by 24 h of exposure to heat-killed *Fn* (HKFn). Data are plotted as mean ± SD and one-way ANOVA with post-hoc *Tukey's* test was performed, n = 4: $^{*}p < 0.5$, $^{**}p < 0.01$, $^{***}p < 0.001$, $^{****}p < 0.0001$.

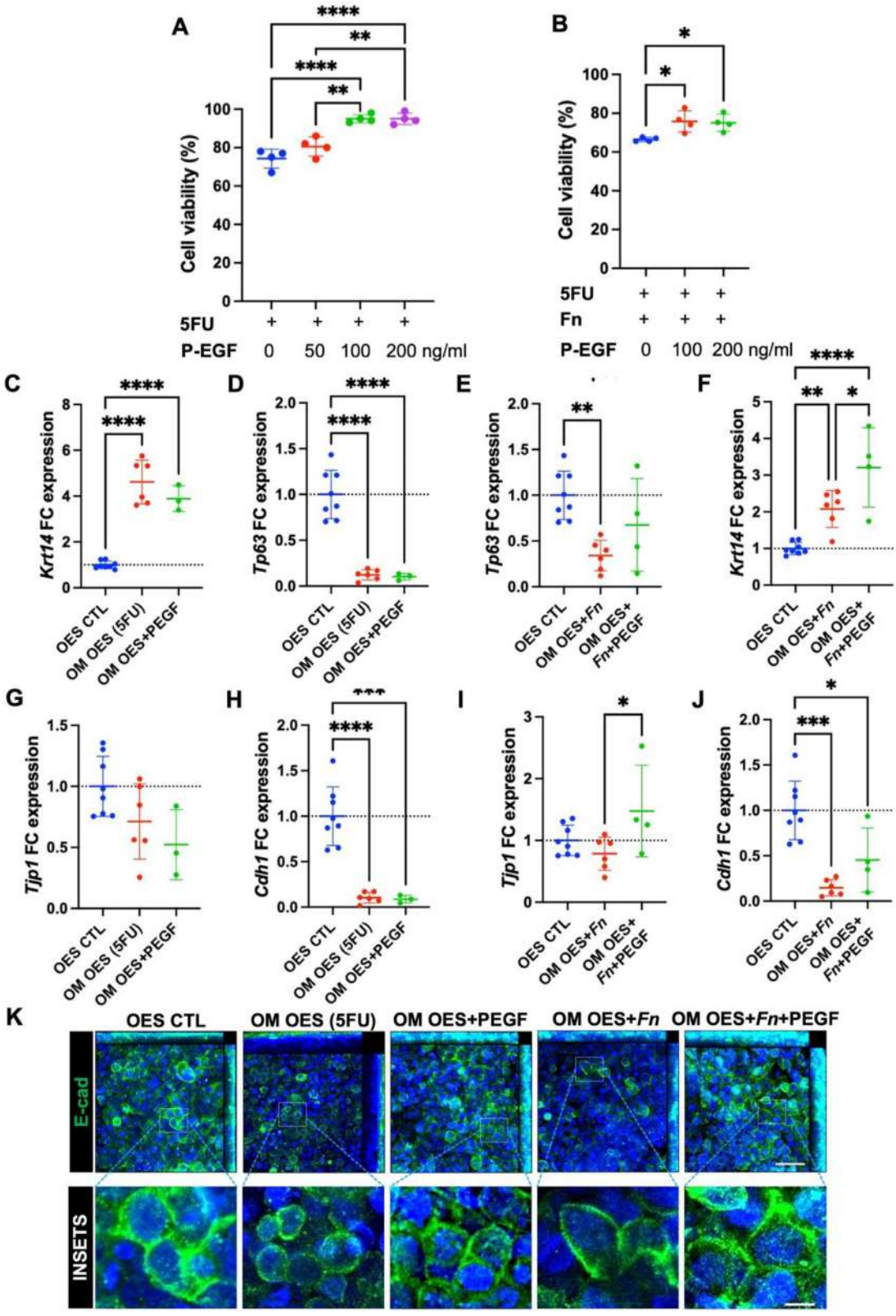

Fig. 4. Protective effects of P-EGF treatment in the OM model with and without *Fn* exposure. (A-B) Viability of OM-like OES in the presence of 5FU (to induce chemotherapy-like treatment), P-EGF treatment only, and P-EGF treatment upon exposure to *Fn*. Data are displayed as mean ± SD and one-way ANOVA, post hoc *Tukey's* test was performed, n = 4: $^{*}p < 0.5$, $^{**}p < 0.01$, $^{****}p < 0.0001$. (**C-J**) Gene expression in OES control (CTL) and OM-like OES (post-treated with 5FU) after P-EGF treatment with or without *Fn* exposure, which was determined by qPCR where fold change was normalized to the house keeping gene *Rps29*. Data are plotted as mean ± SD and one-way ANOVA, post hoc *Tukey's* test was performed, n = 3-8: $^{*}p < 0.5$, $^{**}p < 0.01$, $^{***}p < 0.001$, *** $p < 0.0001$. (**K**) Maximum intensity projections with sidelined XYZ orthogonal projections from confocal microscopy z-stacks showing E-cadherin (Ecad) expression in: untreated OES, OM-associated OES treated with 5FU only, OM-associated OES treated with P-EGF or *Fn* or *Fn*+P-EGF. Scale bar of top row micrographs: 50 μm. Scale bar in insets: 50 μm. For the quantification plots of E-cadherin protein and mRNA in all groups, the reader should look at Figure S4 in the supplementary materials file.

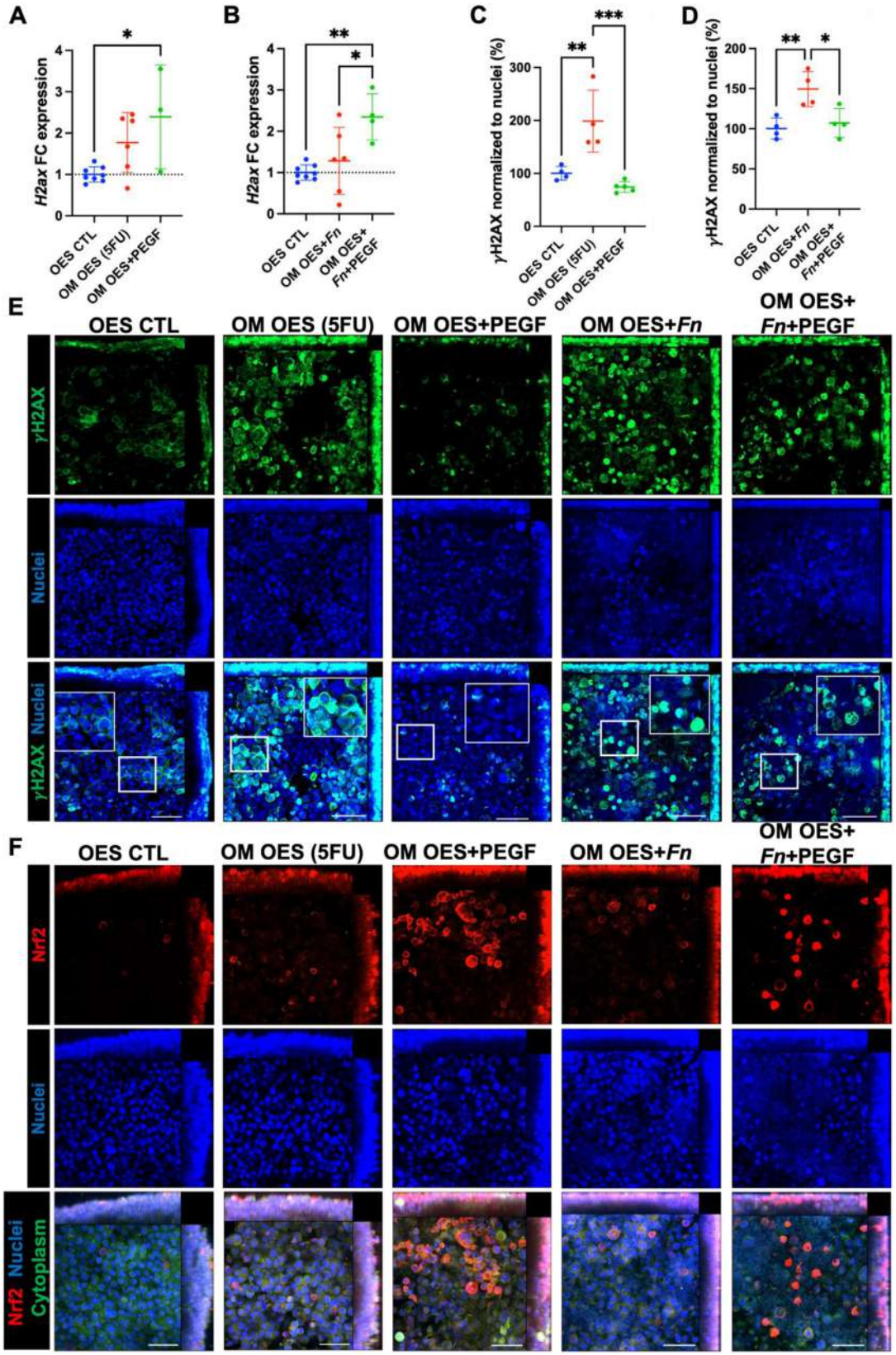

Fig. 5. P-EGF protective effects are mediated by inhibition of DNA strand breaks and oxidative stress. (A, B) Gene expression of DNA strand breaks marker, *H2ax*, using qPCR. Data are displayed as mean ± SD and one-way ANOVA, post hoc *Tukey's* test was performed, n = 3-8: $^{*}p < 0.5$, $^{**}p < 0.01$. (**C, D**) Quantitative analysis of $\gamma H2AX$ to evaluate DNA double-strand break repair. Data are plotted as mean ± SD and one-way ANOVA, post hoc *Tukey's* test was performed, n = 4, $^{*}p < 0.5$, $^{***}p < 0.001$, $^{****}p < 0.0001$ (**E, F**). Maximum intensity projection confocal micrographs sidelined with XYZ orthogonal projections for γH2AX and Nrf2 and counterstained the nuclear Hoechst and with a cytoplasm dye for investigating Nrf2 nuclear translocation. White frames indicate areas of DNA strand break repair. Scale bar: 50 μm.

gene expression and acute release of pro-inflammatory cytokines was assessed. P-EGF at 200 ng/ml significantly reduced the expression of *Il-8* and *Il-1β* (Fig. 6A-D). Conversely, P-EGF treatment appeared to promote the release of IL-6 and IL-8 cytokines to the conditioned media, particularly with 200 ng/ml dose and less markedly with 100 ng/ml (Fig. 6E-F), but without statistical significance.

Migration of oral epithelial cells in the OM model within the millifluidic integrated system was assessed using an *in vitro* transwell set up. P-EGF administration significantly enhanced epithelial migration in the OM models. Although OM models (5FU-treated) generally had a diminished cell migration, subsequent treatment with P-EGF was able to restore it to normal levels (Fig. 6G, H). Interestingly, similar patterns were observed in OM models without and with the exposure to *Fn* after P-EGF administration (Fig. 6G, I).

Overall, these outcomes suggest that P-EGF had beneficial effects on epithelial cell migration and suppressing oxidative stress, yet its direct influence is limited in the acute release of pro-inflammatory cytokines into microenvironment despite remarkable changes at the transcriptomic level.

3.5. P-EGF promoted calcium-dependent epithelial function in OM under Fn exposure

Intracellular calcium mobilization and metabolism following damage of epithelial linings is known to involve cellular signals associated with wound repair [28]. Therefore, an intracellular calcium influx assay was performed to evaluate calcium influx in OES and OM models. OES and OM models were transferred to the millifluidic platform for mimicking metabolic flow and pharmacodynamics. Immediately after the wound scraping was performed in normal OES models, an increase in intracellular calcium was observed (Fig. 7A). However, OM models exhibited a diminished calcium response, suggesting a deleterious effect of the chemotherapeutic agent (5FU) on calcium-dependent cellular signaling (Fig. 7A). P-EGF administration was found to partially restore calcium signaling, showing its potential to mitigate the impact of 5FU in OM models (Fig. 7A-B). Notably, P-EGF administration did enhance calcium signaling in OM even upon *Fn* exposure, although the levels were slightly lower than those observed in P-EGF-treated OM without *Fn* (Fig. 7A-C).

Taken together, these findings indicate that P-EGF therapeutic administration facilitated epithelial intracellular calcium metabolism while partially reversing the cytotoxicity induced by 5FU in OM models. Despite such effects, *Fn* could negatively modulate such metabolism.

4. Discussion

In this study, our research team successfully developed bioprinted OES and CT-induced OM models in static and dynamic millifluidic OM systems. More importantly, these disease models were amenable to the exposure of a specific OM pathogenic bacteria (*Fn*) to investigate the effectiveness of a promising plant molecular farming therapeutic cue in the epithelial interface in the presence of a salivary pathogen. Since one of our research groups has shown promising re-epithelization outcomes with *Nicotiana benthamiana* plant-produced EGF (P-EGF), here, we showed that it could also enhance epithelial repair in OM models within millifluidic systems.

Firstly, an OES model was assembled using M3DB nanotechnology within a relatively short time (6 days), which expressed specific epithelial phenotypic markers, mainly basal, for targeting drug screening and discovery targeting CT-induced OM. Clinically, the shorter biofabrication time of our OES model accelerates the drug screening process, allowing for a quicker identification of optimal therapies for oral diseases such as OM. This rapid production enhances the efficiency of screening therapeutic candidates, offering a timelier approach to cancer treatment and drug discovery. OES tissue constructs formed in dynamic millifluidic systems showed more robust epithelial tissue barrier characteristics/functions intrinsic to oral epithelial tissue equivalents compared to the static ones. Magnetic nanoparticles (MNP) have been widely applied in 3D bioprinting to generate organoids of brain [29], lacrimal gland [30], salivary gland [18] and intestine [31] within a relatively short culture duration compared to traditional methods. These MNP do not appear to affect cell viability or trigger inflammation and oxidative stress responses [32]. Also, this bioprinting platform is a consistent, scaffold-free platform that can enhance efficiency of organoid formation [30]. In our study, an OES model was formed by this magnetic bioassembly technique and showed features of a nonkeratinized stratified squamous epithelium in less than one week, while conventional methods using insert and lifting keratinocytes to air-liquid interface need 2-3 weeks for cells to differentiate and form a multilayered tissue construct [33–35]. Interestingly, our bioprinted OES model achieved a thickness of 80 ±5 μm, closely resembling the 99 μm thickness reported at the floor of the mouth [36], which is one of the most affected sites in CT-induced OM [37]. Herein, oral keratinocytes were spatially assembled into a sheet-like shape under the driving force of a magnetic field, facilitating epithelial cell-cell adhesion and compaction with limited cell differentiation as per the abundant presence of mitotic basal K14 and p63 progenitors but with signs of epithelial stratification (Figs. 1E, 2F, S1). This limited differentiated status is usually maintained in microfluidic platforms providing a dynamic fluid flow with lack of full keratinocyte differentiation and stratification [38]. By using a peristaltic pump device, the dynamic millifluidic system (MIVO®) was enabled after this bioprinted OES tissue construct was carried and transferred with a transwell insert into a millifluidic chamber to create a laminar flow interface for 5FU CT drug perfusion and to facilitate the interaction between *Fn*, the critical OM pathogen, and bioprinted oral epithelium to enable drug discovery. Our interface set up takes advantage of physiological fluid flow microenvironments in terms of nutrient supply and metabolic waste elimination, thus enhancing the cell viability of OES (Fig. 1F). A controlled dynamic fluid can provide more realistic and physiologically relevant microenvironments that better mimic in vivo conditions, and its advantages were confirmed in a previous report when efficacy of anti-cancer drugs was determined using this dynamic system [20]. This report demonstrated that drug diffusion in dynamic conditions is better than static, and drug administration was more closely mirrored the in vivo scenario. This dynamic system was also previously used on skin epithelial models to test penetration of skin upon the administration of different molecules [19]. Yet, optimization of fluid flow velocity is also relevant as a flow rate of 10 mm/s promoted an improved cell viability when compared to 5 mm/s or 20 mm/s (Fig. S2). The Trypan blue exclusion method was used to determine cell viability after trypsinization of the OES, since it has been reported to be a reliable method for assessing that specific outcome [39]. Other experimental approaches such as ATP-luciferase-based 3D assays were performed, however, the outcomes were inconsistent in the both control and experimental groups, likely due to the high cell density present in the OES.

Secondly, these models were used to create CT-induced OM models in the presence of *Fn*. The rescuing effects of P-EGF on OM-like OES models exposed to the *Fn* stimuli were investigated. Mimicking the clinical dose of the CT drug 5FU is challenging due to variations in dosing which depend on tumor types, organs, and whether the tumor is primary, recurrent, or metastatic [40]. For example, one study reported that the 5FU plasma concentration peaked at 650 ng/ml [41]. However, 5FU at low dose (5 μg/ml) had minimal impact on OES viability, prompting the selection of a significantly higher dose (500 μg/ml) alike other studies [34]. This high 5FU dose led to an increased release of pro-inflammatory cytokines, disruption of cell-cell communications and elevated γH2AX accumulation (Figs. 3 and 4). The upregulation of IL-6 and IL-8 and reduced E-cadherin were reportedly associated with oral mucositis [21,42]. The accumulation of γH2AX is indicative double-strand DNA breaks and repair [43]. As an analogue of uracil, 5FU is known to disrupt DNA replication and RNA synthesis by misincorporation of fluorouridine nucleotides and inhibiting enzyme thymidylate

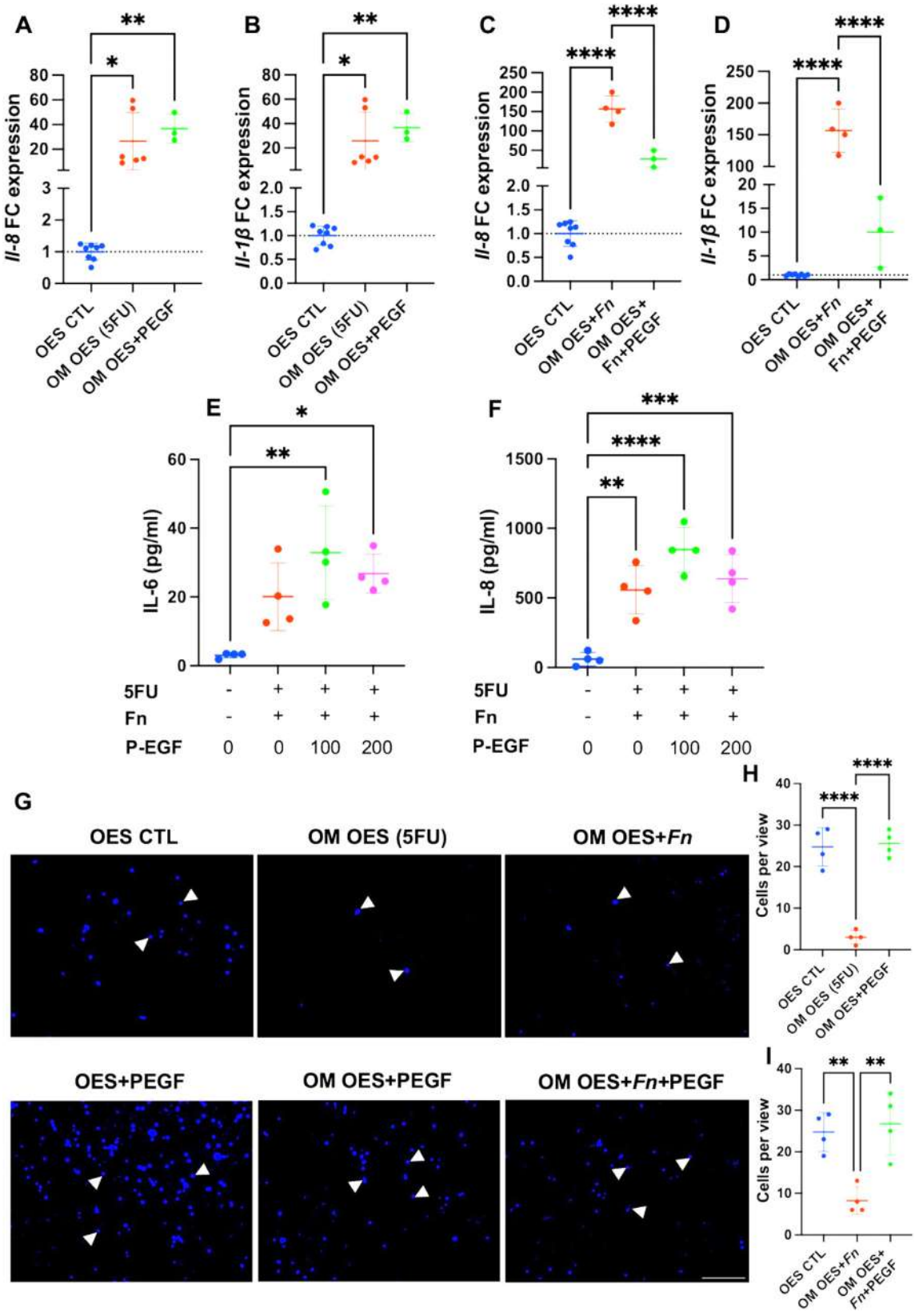

Fig. 6. Treatment efficacy of P-EGF in modulating pro-inflammatory cytokine expression and cell migration in the OM model within the millifluidic system. (A-F) expression of pro-inflammatory cytokine at mRNA level via qPCR (A-D) and protein level by ELISA (E-F). Data are plotted as mean ± SD and one-way ANOVA with post-hoc *Tukey*'s test was performed. $^{*}p < 0.5$, $^{**}p < 0.01$, $^{****}p < 0.0001$. **(G-I)** Epithelial cell migration in the OM model was assessed by transwell migration assay and visualized by fluorescent microscopy at magnification of 20X and respective quantification using ImageJ. White arrowheads indicate the nuclei of migrating cells, which were stained with Hoechst 33342. Scale bar: 100 μm. Data are displayed as mean ± SD and one-way ANOVA with post-hoc *Tukey*'s test was performed, n = 4: $^{**}p < 0.01$, $^{****}p < 0.0001$.

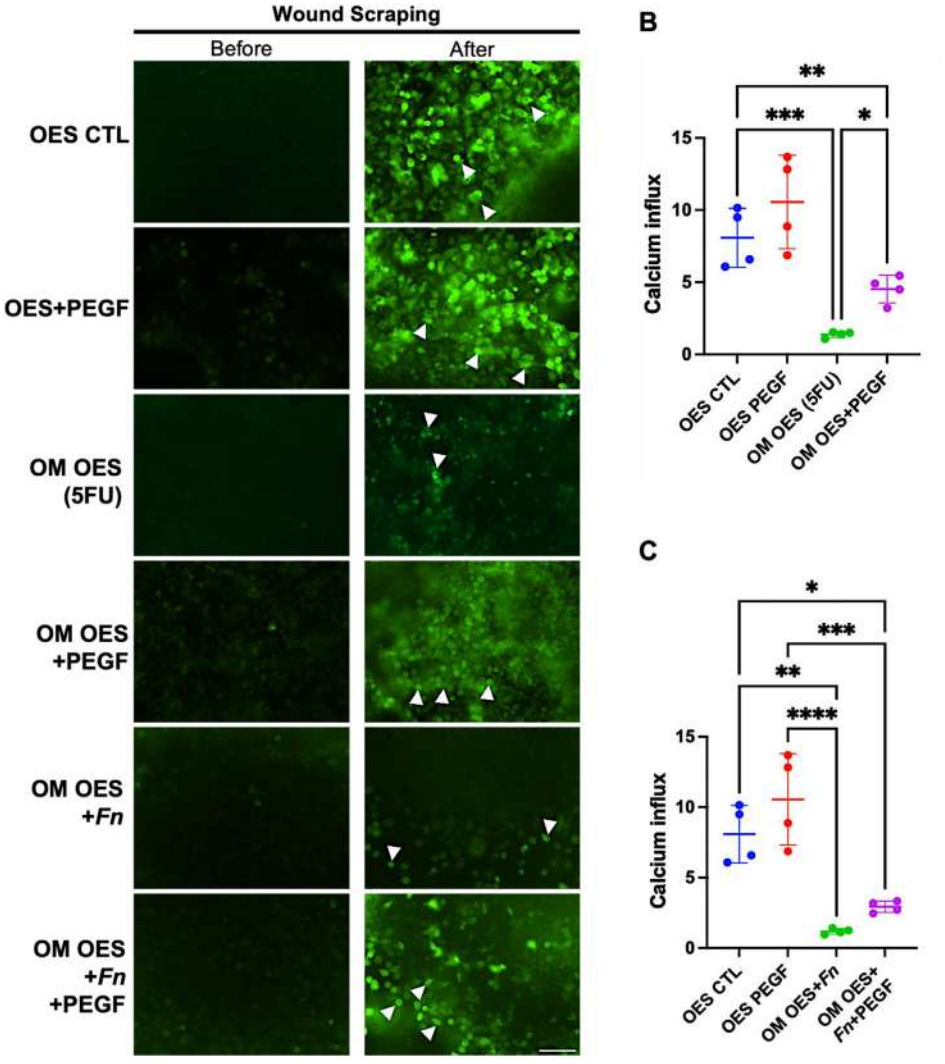

Fig. 7. Intracellular calcium mobilization in the OES tissue construct in the OM model within the millifluidic system during P-EGF treatment before and after wound scraping. OES in the OM model were wound-scraped for assessment of intracellular calcium influx. (**A**) Micrographs were acquired with a fluorescent microscope and compressed at maximum intensity projections after z-stacking. White arrowheads indicate the cells with increasing calcium influx signals after wound scraping. Mag.: 20X, Scale bar: 100 μm. (**B-C**) Quantified by ImageJ, Data are displayed as mean ± SD and one-way ANOVA with post-hoc *Tukey's* test was performed, n = 4. $^{*}p < 0.5$, $^{**}p < 0.01$, $^{***}p < 0.001$, $^{****}p < 0.0001$.

synthase synthesis [44]. The observed upregulation of γH2AX in OES after 5FU cytotoxic exposure (alike in CT) reflects the nature of 5FU-induced DNA damage. Although increased γH2AX was noted in 2D cultures of primary oral keratinocytes following irradiation [45], no studies have yet reported on this marker in any 3D models or tissues from OM patients. Nevertheless, higher γH2AX expression in lymphocytes and peripheral blood samples of patients correlates with more severe OM [46,47]. Therefore, our OM-like model created from 5FU-treated OES constructs was robust and reliable.

Fusobacterium nucleatum can become an opportunistic pathogen contributing to the severity of inflammatory diseases. For example, high levels of *Fn* have been reported in patients with OM [6,48]. Infection with *Fn* in oral epithelial cells commonly triggers the release of pro-inflammatory cytokines, including IL-6, IL-8 and IL-1β [49–51]. Using heat-killed bacteria in our experimental set up allowed for controlled dosing and uniformed distribution of circulating bacterial components. In addition, anaerobic conditions cannot be replicated for *Fn* survival, which could not be maintained due to the constant exposure to oxygen in the interconnected chambers of the fluid flow system. The release of IL-6 and IL-8 following exposure to heat-killed *Fn* highlighted the inflammatory responses in OES models (Fig. 3D, E). Future millifluidic platforms could incorporate alternative strategies such as the use of hypoxic media, oxygen-scavenging agents, or integrated oxygen control modules to maintain survival of anaerobic microorganisms like *Fn* in cell culture, creating more physiologically relevant microenvironments to better investigate host–microbe interactions under controlled oxygen gradients.

Since EGF is known to promote the re-epithelization of OM ulcers including epithelial proliferation and migration, plant-produced EGF was used herein to reverse the epithelial damage and assess the inflammatory response in our OM models. High concentration of P-EGF (100 ng/ml) effectively restored the viability of bioprinted OES tissue constructs after CT-induction with 5FU. Despite the presence of *Fn*, which significantly reduced epithelial viability, P-EGF treatment enhanced cell viability, though the improvement was not substantial. These observations were consistent with previous research highlighting P-EGF's role in promoting cell proliferation in both skin keratinocytes and primary salivary gland epithelial cells; yet, notably, these earlier studies did not involve CT cytotoxic exposure [16,52].

From a mechanistic standpoint, our findings reveal that P-EGF decreased the accumulation of γH2AX in our OM models, underscoring its potential to reduce DNA damage and thereby enhancing cell viability and survival. This effect persisted even in the presence of *Fn* in the culture system, demonstrating the robust action of P-EGF. Furthermore, the maintenance of E-cad expression by P-EGF is beneficial in the wound healing process, as E-cadherin-mediated signaling is known to be involved in this biological repair mechanism [53]. This integrated response highlights the multifaceted therapeutic potential of P-EGF in treating CT-damaged epithelial tissues. Moreover, the Nrf2 signaling pathway is known to protect cells from oxidative stress damage

caused by chemotherapeutic drugs and promote the wound healing process [54]. P-EGF administration led to increased Nrf2 activation in our OM models without *Fn* exposure, which was consistent with findings from prior reports, such as the activation of Nrf2 in 5FU-exposed keratinocytes pre-treated with γ-tocotrienol [55] and in mouse models of intestinal mucositis treated with multi-modified stable superoxide dismutase (MS-SOD) [56]. Although Nrf2 nuclear translocation could mitigate oxidative stress induced by *Fn* in oral keratinocytes [57], this is the first study to show that P-EGF can promote nuclear translocation of Nrf2 in oral epithelial tissue constructs exposed to both 5FU cytotoxicity and *Fn*. Activation of Nrf2 appears to facilitate its interaction with nuclear p63 while they are binding to their specific binding regions on DNA, which have been shown to promote keratinocyte proliferation [58], aligning with the observed higher cell viability and survival. Interestingly, while gene expression of pro-inflammatory cytokines was reduced following P-EGF treatment, protein levels in the conditioned media did not show a corresponding decrease. One possible reason relies on the dynamic fluctuations in pro-inflammatory cytokine release and both the timing of media replacement (daily) and the conditioned media collection at endpoint. The current combinatorial set up allows for a cumulative release of those cytokines into the media for less than 24 h, before the media is partially replenished. Consequently, any potential reduction in acute cytokine release, if truly occurred, would not be detectable at early culture times in this experimental setup. This underscores the complexity of cytokine dynamics in response to therapeutic interventions and highlights the importance of considering temporal factors in media replacement (partial or total) in in vitro models to depict changes in cytokine release [59].

The role of P-EGF in inducing cell migration in normal human skin keratinocytes has been reported by one of our researchers [16]. Herein, the cell migration ability was impaired in OM models with and without *Fn* exposure in the epithelial interface when compared to control OES non-disease models in untreated circumstances. Notably, the subsequent administration of P-EGF was able to restore cell migration effectively (100.3 $\pm$ 12 % and 108 $\pm$ 30 %), regardless of the presence of *Fn*. This finding is particularly relevant in the context of OM in patients, where ulcers are prevalent. Enhancing cell migration with P-EGF could significantly aid in the wound healing process, offering a promising therapeutic avenue for improving patient outcomes.

Rapid intracellular calcium response in keratinocytes following an epithelial scratch/scraping represents one of the primary early responses at wound sites, essential for initiating the epithelial healing process and promote re-epithelialization [60]. This healing response generates a wave of increased intracellular calcium ion that spreads outward from the injured area and gradually disappears, mirroring cellular function responding to injury that promotes wound re-epithelialization [61]. Exposure to 5FU in our OM models impairs this calcium ion mobilization or influx response in oral keratinocytes within the OES post-scraping. Importantly, the administration of P-EGF partially reverses the impaired cellular function induced by 5FU in OM models. The role of endogenous calcium extends beyond the prevention of apoptosis as it also supports epithelial migration and proliferation during wound healing [61]. This interplay underscores the potential therapeutic value of P-EGF in enhancing recovery processes in OM models damaged by CT drugs.

It should be noted that the systemic use of a growth factor like EGF could lead to significant and potentially life-threatening side effects, which could promote cancer growth or recurrence [62], particularly if precancerous or cancerous lesions remain post-cancer treatment. Similarly, the use of keratinocyte growth factor (Palifermin, with the tradename Kepivance) is limited to patients with hematologic malignancies due to concerns about its potential to stimulate the growth of non-hematopoietic tumors following systemic delivery [63]. Therefore, the type of P-EGF delivery, particularly the local administration of such epithelial healing factor, is a critical factor in optimizing therapeutic efficacy while minimizing cancer risk. To address this concern, this study administered P-EGF locally over the oral epithelial tissues placed in the chambers of a milifluidic system. Current localized delivery methods such as oral sprays, mouthwashes [64] or intra-oral microneedling patches targeting specific lesions could enhance the therapeutic effectiveness of P-EGF in future studies while maintaining a favorable safety profile [65]. It is also noteworthy that Kepivance is not approved by our local regulatory agencies, which precluded its use as a control in this study.

The therapeutic efficacy of P-EGF may depend on its temporal application, as its timing could influence its ability to modulate inflammation and support tissue repair [66]. In this study, since the ultimate purpose was to treat OM rather than preventing it, P-EGF was administered immediately after 5FU exposure. The high abundance of *Fn* was reported after patients receive chemotherapy [6]; therefore, *Fn* was introduced later after 5FU exposure. Simultaneous administration of P-EGF with the *Fn* bacterial challenge was performed to mimic the clinical scenario of treating OM after oral lesions are present. According to the same studies, *Fn* will only become predominant and pathogenic following chemotherapy. However, administering P-EGF prior to bacterial exposure might yield different outcomes, such as varying levels of protection or enhanced repair mechanisms. Future studies are needed to explore these temporal dynamics if prevention strategies are sought for P-EGF-based therapeutics.

Our study has its limitations. Firstly, our model was perhaps simplistic as it was developed to investigate the biological effects in the interface between the oral epithelia and salivary OM-associated pathogens; hence, the creation of a lamina propria was not considered at this initial step. A lack of a lamina propria layer that contains fibroblasts and extracellular matrix (ECM) is relevant to recapitulate the native oral mucosa as fibroblasts in connective tissue affect keratinocyte proliferation, differentiation and adhesion [21].

The absence of submucosal fibroblasts and macrophages in our culture system could not reflect the dynamic and complex interactions that occur with epithelial cells *in vivo* once OM occurs, especially in the presence of a pathobiont like *Fn*. Oral fibroblasts have been reported to modulate macrophage activity following bacterial infection [67], and immune components such as macrophages and cytokine gradients are known to influence inflammatory responses and tissue repair [68]. However, these complex immune interactions are beyond the scope of this study, but surely must be addressed later on. At the epithelial level, our findings demonstrated that *Fn* intensified the severity of injury in our OM millifluidic models. Although P-EGF did not reduce cytokine release under *Fn* presence, it enhanced cell survival, augmented the expression of cell-cell epithelial junctions, promoted cell migration and wound healing response, reduced DNA damage and mitigated oxidative stress. The involvement of lamina propria and submucosa with other cell types could potentially reveal additional protective effects or amplify tissue damage after P-EGF administration, but at the same time it would increase substantially the complexity of *Fn* interactions and mask crucial epithelial interactions that take place. Future works will incorporate lamina propria and submucosa layers and immune cell interactions to better understand their role in epithelial protection and repair. Additionally, investigations into the role of salivary immune components and proteins at the interface between saliva and the oral epithelia are key to provide a more comprehensive understanding of the dynamics of saliva and immunity in this model.

Despite these limitations, the incorporation of lamina propria to an oral epithelial construct also exhibits drawbacks. For example, if researchers use stiff ECM macromolecules for developing the lamina propria/submucosa layer in microfluidic chips like collagen, the shear stress forces would increase exponentially according to the Hagen–Poiseuille's law due to the narrow channels and circuits present [25,26]. Perhaps this is the reason why Ly and colleagues (2024) did not use any fluid flow set up in their OM microfluidic chips containing a lamina propria with photo-crosslinked collagenous ECM construct with both epithelial and submucosal layers with gingival keratinocytes, fibroblasts and endothelial cells [24]. A poor oral stratified epithelia was displayed in this

bioassembled triculture tissue study aiming for an OM model on a chip. Millifluidic cell culture platforms offer relevant advantages for disease modeling in comparison with microfluidic chips, since these platforms facilitate a more accurate drug diffusion, improve mass transport, promote cell differentiation and are more resistant to chemicals [25,26] The use of airlifting oral gingiva cultures, composed of oral keratinocytes and gingival fibroblasts, in large triple chamber microfluidic systems (by REVIVO Biosystems) can provide an effective diffusion area of 0.4 cm^2 with the assistance of a peristaltic pump [69]. Despite these endeavors, these gingival tissue equivalents are still not comparable to the actual thickness of the human gingiva, and researchers have not yet assessed the use of systemic drugs, for chemotherapy for example, in their system. One should note that endothelial cells in the submucosa were not included in this latter study, and these as well as fibroblasts are relevant in host-pathogen interactions but only following epithelial breakdown during OM pathogenesis.

In this study, our focus was solely on *Fn*, despite the oral cavity harboring hundreds of different microbial species. Exploring the roles of other prevalent bacterial pathogens in OM, such as *Prevotella* spp. or using bacterial biofilms is an interesting direction to be pursued [5,70]. Further research will aim to integrate these components to provide a more comprehensive understanding of the impact of the oral microbiome as well as the collective oralome on the pathogenesis and management of CT-induced OM.

Our OES interface model offers a promising potential for precision oncology. For example, it could be used as a drug screening platform in OM prior to cancer therapy, by providing a more predictive tool for evaluating the biological and cytotoxic effects of both 5-FU and OM therapeutic agents in oral epithelia. In addition, it could serve as an effective platform for studying host-pathogen interactions in the oral epithelia. As the oral microbiome plays an important role in the development and progression of OM, elucidating these interactions would shed lights on OM pathogenesis and could lead to novel microbiome-based interventions, such as probiotics, prebiotics, and postbiotics [71]. The OES model could also be valuable in testing for efficacy and epithelial cytotoxicity of these novel interventions and other oral care products. These applications highlight the clinical relevance and translational potential of our millifluidic interface in advancing precision oncology and oral healthcare.

5. Conclusion

In summary, a physiologically relevant oral epithelium 3D sheet-like construct and an OM disease model were created within a relative short time inside a tissue culture system under static and dynamic millifluidic conditions. The OM model was meaningful to confirm the alleviating effects of P-EGF on the oral epithelia exposed to 5FU chemotherapeutic drug in the presence of OM-associated pathogen, *Fn.* Taken together, the outcomes indicate that P-EGF can rescue the epithelial viability, resolve DNA repair, mitigate cellular oxidative stress, promote cell migration and restore intracellular calcium metabolism in OM models regardless of *Fn* exposure in these millifluidic platforms. These dynamic OM models also reconfirm P-EGF as a promising therapeutic modality to speed up oral re-epithelialization and wound healing upon local delivery.

Ethics statement

All methods were carried out in accordance with relevant local guidelines and regulations, and in accordance with the Declaration of Helsinki. This study did not involve any type of in vivo experimentation in live vertebrates and no human tissue specimens were used. All in vitro studies conducted with the human normal oral keratinocyte cell line (NOK) were approved by the Human Research Ethics Committee of the Faculty of Dentistry, Chulalongkorn University, Bangkok, Thailand (certificate number: HREC-DCU 2023-022, approved on March 31, 2023).

Conflict of interest statement

Silvia Scaglione is an employee and shareholder of React4life company, which is manufacturing the MIVO millifluidic system. Glauco R. Souza is the Co-Founder, Director and member of the Board of Directors of ChemoSen3D. In addition, Glauco R. Souza is the Director of Global Business Development and Innovation at Greiner Bio-one (GBO), which manufactures the magnetic 3D cell culture and the Nanoshuttle magnetic nanoparticles.

CRediT authorship contribution statement

Tien T.T. Truong: Writing – review & editing, Writing – original draft, Visualization, Methodology, Investigation, Formal analysis, Conceptualization. **Toan V. Phan:** Writing – review & editing, Writing – original draft, Visualization, Methodology, Investigation, Formal analysis, Conceptualization. **Yamin Oo:** Writing – review & editing, Writing – original draft, Methodology, Investigation, Formal analysis. **Ladawan Sariya:** Writing – review & editing, Writing – original draft, Validation, Resources, Methodology, Investigation, Formal analysis. **Risa Chaisuparat:** Writing – review & editing, Writing – original draft, Visualization, Validation, Supervision, Resources, Methodology, Funding acquisition. **Silvia Scaglione:** Writing – review & editing, Writing – original draft, Resources, Methodology, Conceptualization. **Glauco R. Souza:** Writing – review & editing, Writing – original draft, Resources, Methodology. **Supansa Yodmuang:** Writing – review & editing, Resources, Methodology, Funding acquisition, Conceptualization. **Catherine H.L. Hong:** Writing – review & editing, Visualization, Funding acquisition, Conceptualization. **Kai Soo Tan:** Writing – review & editing, Visualization, Methodology, Funding acquisition, Conceptualization. **Waranyoo Phoolcharoen:** Writing – review & editing, Resources, Methodology, Funding acquisition, Conceptualization. **Oranart Matangkasombut:** Writing – review & editing, Writing – original draft, Visualization, Validation, Supervision, Resources, Methodology, Investigation, Funding acquisition, Conceptualization. **João N. Ferreira:** Writing – review & editing, Writing – original draft, Visualization, Validation, Supervision, Software, Resources, Project administration, Funding acquisition, Formal analysis, Data curation, Conceptualization.

Acknowledgements

This project is funded by the National Research Council of Thailand (NRCT) and Chulalongkorn University with project number: N42A670176 to JNF (main PI) and to RC (Co-I). This study is partially supported by the International Association for Dental, Oral and Craniofacial Research (IADR) 2022 Innovation in Oral Care Award funded by GlaxoSmithKline to JNF, CHLH, KST, SY and WP. This project is also supported by Thailand Science Research and Innovation Fund Chulalongkorn University to JNF and RC. Center of Excellence and Innovation for Oral Health and Healthy Longevity is funded by the Ratchadaphiseksomphot Endowment Fund, Chulalongkorn University (Grant number: CE68_003_3200_001). TTTT studies were supported by a Chulalongkorn University scholarship from Graduate Scholarship Program for ASEAN or Non-ASEAN Countries. The graduate student's research work is supported by the 90th Anniversary of Chulalongkorn University Scholarship under Ratchadapisek Somphot Endowment Fund (Grant number: GCUGR1125662098M) and by the IADR-Southeast Asia Mentor-Mentee Funding provided to TTTT under the mentorship of JNF and OM. This research project is supported by the Second Century Fund (C2F), Chulalongkorn University provided to TVP. The funders had no role in study design, data collection and analysis, decision to publish, or preparation of the manuscript. We would like to give a special thanks to Mr. Somchai Yodsanga from Department of Oral Pathology for the assistance to prepare and stain the tissue sections for histology.

Supplementary materials

Supplementary material associated with this article can be found, in the online version, at doi:10.1016/j.engreg.2025.02.001.

References

[1] K. Berger, D. Schopohl, A. Bollig, D. Strobach, C. Rieger, D. Rublee, H. Ostermann, Burden of oral mucositis: a systematic review and implications for future research, Oncol. Res. Treatment 41 (6) (2018) 399–405.

[2] S. Elad, N. Yarom, Y. Zadik, M. Kuten-Shorrer, S.T. Sonis, The broadening scope of oral mucositis and oral ulcerative mucosal toxicities of anticancer therapies, CA: Cancer J. Clin. 72 (1) (2022) 57–77.

[3] N. Gupta, S.Y. Quah, J.F. Yeo, J. Ferreira, K.S. Tan, C.H.L. Hong, Role of oral flora in chemotherapy-induced oral mucositis in vivo, Arch. Oral Biol. 101 (2019) 51–56.

[4] J. Hou, H. Zheng, P. Li, H. Liu, H. Zhou, X. Yang, Distinct shifts in the oral microbiota are associated with the progression and aggravation of mucositis during radiotherapy, Radiother. Oncol. 129 (1) (2018) 44–51.

[5] A. Vesty, K. Gear, K. Biswas, B.W. Mackenzie, M.W. Taylor, R.G. Douglas, Oral microbial influences on oral mucositis during radiotherapy treatment of head and neck cancer, Support. Care Cancer 28 (6) (2020) 2683–2691.

[6] B.-Y. Hong, T. Sobue, L. Choquette, A.K. Dupuy, A. Thompson, J.A. Burleson, A.L. Salner, P.K. Schauer, P. Joshi, E. Fox, Chemotherapy-induced oral mucositis is associated with detrimental bacterial dysbiosis, Microbiome 7 (1) (2019) 1–18.

[7] M. Zepeda-Rivera, S.S. Minot, H. Bouzek, H. Wu, A. Blanco-Miguez, P. Manghi, D.S. Jones, K.D. LaCourse, Y. Wu, E.F. McMahon, S.N. Park, Y.K. Lim, A.G. Kempchinsky, A.D. Willis, S.L. Cotton, S.C. Yost, E. Sicinska, J.K. Kook, F.E. Dewhirst, N. Segata, S. Bullman, C.D. Johnston, A distinct Fusobacterium nucleatum clade dominates the colorectal cancer niche, Nature 628 (8007) (2024) 424–432.

[8] S. Elad, K.K.F. Cheng, R.V. Lalla, N. Yarom, C. Hong, R.M. Logan, J. Bowen, R. Gibson, D.P. Saunders, Y. Zadik, MASCC/ISOO clinical practice guidelines for the management of mucositis secondary to cancer therapy, Cancer 126 (19) (2020) 4423–4431.

[9] P. Rousselle, F. Braye, G. Dayan, Re-epithelialization of adult skin wounds: cellular mechanisms and therapeutic strategies, Adv. Drug Deliv. Rev. 146 (2019) 344–365.

[10] J. Coutsouvelis, C. Corallo, A. Spencer, S. Avery, M. Dooley, C.M. Kirkpatrick, A meta-analysis of palifermin efficacy for the management of oral mucositis in patients with solid tumours and haematological malignancy, Crit. Rev. Oncol./Hematol. 172 (2022) 103606.

[11] P.W. Finch, L.J. Mark Cross, D.F. McAuley, C.L. Farrell, Palifermin for the protection and regeneration of epithelial tissues following injury: new findings in basic research and pre-clinical models, J. Cell. Mol. Med. 17 (9) (2013) 1065–1087.

[12] J. Chen, L.A. Bekale, K.M. Khomtchouk, A. Xia, Z. Cao, S. Ning, S.J. Knox, P.L. Santa Maria, Locally administered heparin-binding epidermal growth factor-like growth factor reduces radiation-induced oral mucositis in mice, Sci. Rep. 10 (1) (2020) 17327.

[13] H.G. Wu, S.Y. Song, Y.S. Kim, Y.T. Oh, C.G. Lee, K.C. Keum, Y.C. Ahn, S.w. Lee, Therapeutic effect of recombinant human epidermal growth factor (RhEGF) on mucositis in patients undergoing radiotherapy, with or without chemotherapy, for head and neck cancer: a double-blind placebo-controlled prospective phase 2 multi-institutional clinical trial, Cancer: Interdiscipl. Int. J. Am. Cancer Soc. 115 (16) (2009) 3699–3708.

[14] A. Bhatwa, W. Wang, Y.I. Hassan, N. Abraham, X.-Z. Li, T. Zhou, Challenges associated with the formation of recombinant protein inclusion bodies in Escherichia coli and strategies to address them for industrial applications, Front. Bioeng. Biotechnol. 9 (2021) 630551.

[15] B. Shanmugaraj, C.J.I. Bulaon, W. Phoolcharoen, Plant molecular farming: a viable platform for recombinant biopharmaceutical production, Plants 9 (7) (2020) 842.

[16] O. Hanittinan, Y. Oo, C. Chaotham, K. Rattanapisit, B. Shanmugaraj, W. Phoolcharoen, Expression optimization, purification and in vitro characterization of human epidermal growth factor produced in Nicotiana benthamiana, Biotechnol. Rep. 28 (2020) e00524.

[17] T.T.T. Truong, T.V. Phan, Y. Oo, W. Phoolcharoen, O. Matangkasombut, J.N. Ferreira, Nicotiana benthamiana-derived epidermal growth factor rescues human oral keratinocytes exposed to 5-fluorouracil cytotoxicity, Mahidol Dent. J. [Internet] 43 (2023) S67–S76.

[18] C. Adine, K.K. Ng, S. Rungarunlert, G.R. Souza, J.N. Ferreira, Engineering innervated secretory epithelial organoids by magnetic three-dimensional bioprinting for stimulating epithelial growth in salivary glands, Biomaterials 180 (2018) 52–66.

[19] I. Pulsoni, M. Lubda, M. Aiello, A. Fedi, M. Marzagalli, J. von Hagen, S. Scaglione, Comparison between Franz diffusion cell and a novel micro-physiological system for in vitro penetration assay using different skin models, SLAS Technol. 27 (3) (2022) 161–171.

[20] A. Marrella, G. Varani, M. Aiello, I. Vaccari, C. Vitale, M. Mojzisek, C. Degrassi, S. Scaglione, 3D fluid-dynamic ovarian cancer model resembling systemic drug administration for efficacy assay, ALTEX-Altern. Anim. Exp. 38 (1) (2021) 82–94.

[21] T. Sobue, M. Bertolini, A. Thompson, D.E. Peterson, P.I. Diaz, A. Dongari-Bagtzoglou, Chemotherapy-induced oral mucositis and associated infections in a novel organotypic model, Mol. Oral Microbiol. 33 (3) (2018) 212–223.

[22] E. Barker, L. AlQobaly, Z. Shaikh, K. Franklin, J. Thurlow, B. Moghaddam, J. Pratten, K. Moharamzadeh, Biological evaluation of oral care products using 3D tissue-engineered in vitro models of plaque-induced gingivitis, Dent. J. (Basel) 12 (5) (2024).

[23] K.L. Ly, X. Luo, C.B. Raub, Oral mucositis on a chip: modeling induction by chemo- and radiation treatments and recovery, Biofabrication 15 (1) (2022).

[24] K.L. Ly, M. Rajtboriraks, A. Elgerbi, X. Luo, C.B. Raub, Recombinant human keratinocyte growth factor ameliorates cancer treatment-induced oral mucositis on a chip, Adv. Healthc. Mater. 13 (14) (2024) e2302970.

[25] L. Chen, C. Yang, Y. Xiao, X. Yan, L. Hu, M. Eggersdorfer, D. Chen, D.A. Weitz, F. Ye, Millifluidics, microfluidics, and nanofluidics: manipulating fluids at varying length scales, Mater. Today Nano 16 (2021) 100136.

[26] J.M. Wilkinson, A review of complex in vitro cell culture stressing the importance of fluid flow and illustrated by organ on a chip liver models, Front. Toxicol. 5 (2023) 1170193.

[27] R.M. Castilho, C.H. Squarize, K. Leelahavanichkul, Y. Zheng, T. Bugge, J.S. Gutkind, Rac1 is required for epithelial stem cell function during dermal and oral mucosal wound healing but not for tissue homeostasis in mice, PLoS One 5 (5) (2010) e10503.

[28] J.V. Cordeiro, A. Jacinto, The role of transcription-independent damage signals in the initiation of epithelial wound healing, Nat. Rev. Mol. Cell Biol. 14 (4) (2013) 249–262.

[29] H. Kim, Y.-J. Lee, Y. Kwon, J. Kim, Efficient generation of brain organoids using magnetized gold nanoparticles, Sci. Rep. 13 (1) (2023) 21240.

[30] T. Rodboon, S. Yodmuang, R. Chaisuparat, J.N. Ferreira, Development of high--throughput lacrimal gland organoid platforms for drug discovery in dry eye disease, SLAS Discov. 27 (3) (2022) 151–158.

[31] L. Xian, L. Chia, D. Georgess, L. Luo, S. Shuai, A.J. Ewald, L.M. Resar, Genetic engineering of primary mouse intestinal organoids using magnetic nanoparticle transduction viral vectors for frozen sectioning, JoVE (J. Visualiz. Exp.) (147) (2019) e57040.

[32] H. Tseng, J.A. Gage, T. Shen, W.L. Haisler, S.K. Neeley, S. Shiao, J. Chen, P.K. Desai, A. Liao, C. Hebel, A spheroid toxicity assay using magnetic 3D bioprinting and real-time mobile device-based imaging, Sci. Rep. 5 (1) (2015) 13987.

[33] K. de Carvalho Dias, D.L. de Sousa, P.A. Barbugli, P.S. Cerri, V.M. Salih, C.E. Vergani, Development and characterization of a 3D oral mucosa model as a tool for host-pathogen interactions, J. Microbiol. Meth. 152 (2018) 52–60.

[34] T. Sobue, M. Bertolini, A. Thompson, A. Dongari-Bagtzoglou, Model of chemotherapy-associated mucositis and oral opportunistic infections, Bio-Protocol 9 (21) (2019) e3411 -e3411.

[35] S.J. Gould, A.D. Foey, V.M. Salih, An organotypic oral mucosal infection model to study host-pathogen interactions, J. Tissue Eng. 14 (2023) 20417314231197310.

[36] S. Prestin, S.I. Rothschild, C.S. Betz, M. Kraft, Measurement of epithelial thickness within the oral cavity using optical coherence tomography, Head Neck 34 (12) (2012) 1777–1781.

[37] M. de Pauli Paglioni, K.M. Faria, N.R. Palmier, A.C. Prado-Ribeiro, E.D. RB, H. da Graca Pinto, N.S. Treister, J.B. Epstein, C.A. Migliorati, A.R. Santos-Silva, T.B. Brandao, Patterns of oral mucositis in advanced oral squamous cell carcinoma patients managed with prophylactic photobiomodulation therapy-insights for future protocol development, Lasers Med. Sci. 36 (2) (2021) 429–436.

[38] M. Rahimnejad, H. Makkar, R. Dal-Fabbro, J. Malda, G. Sriram, M.C. Bottino, Biofabrication strategies for oral soft tissue regeneration, Adv. Healthc. Mater. (2024) 2304537.

[39] F. Piccinini, A. Tesei, C. Arienti, A. Bevilacqua, Cell counting and viability assessment of 2D and 3D cell cultures: expected reliability of the trypan blue assay, Biol. Proced. Online 19 (2017) 8.

[40] J.J. Lee, J.H. Beumer, E. Chu, Therapeutic drug monitoring of 5-fluorouracil, Cancer Chemother. Pharmacol. 78 (3) (2016) 447–464.

[41] M. Terashima, T. Irinoda, H. Kawamura, A. Takagane, K. Abe, K. Oyama, H. Fujiwara, K. Saito, M. Gotoh, T. Shirasaka, Intermittent FLDP: 24-h infusion of 5-FU on days 1, 3 and 5 combined with low-dose cisplatin on days 1–5 for gastric cancer, and its pharmacologic and kinetic rationale, Cancer Chemother. Pharmacol. 51 (2003) 240–246.

[42] M. Bertolini, T. Sobue, A. Thompson, A. Dongari-Bagtzoglou, Chemotherapy induces oral mucositis in mice without additional noxious stimuli, Transl. Oncol. 10 (4) (2017) 612–620.

[43] I. Revet, L. Feeney, S. Bruguera, W. Wilson, T.K. Dong, D.H. Oh, D. Dankort, J.E. Cleaver, Functional relevance of the histone gammaH2Ax in the response to DNA damaging agents, Proc. Natl. Acad. Sci. U. S. A. 108 (21) (2011) 8663–8667.

[44] D.B. Longley, D.P. Harkin, P.G. Johnston, 5-fluorouracil: mechanisms of action and clinical strategies, Nat. Rev. Cancer 3 (5) (2003) 330–338.

[45] A.R. Thomsen, C. Aldrian, B. Luka, S. Hornhardt, M. Gomolka, S. Moertl, J. Hess, H. Zitzelsberger, T. Heider, N. Schlueter, S. Rau, B.M. Ordonez, H. Schafer, G. Rucker, M. Henke, Biopsy-derived oral keratinocytes - a model to potentially test for oral mucosa radiation sensitivity, Clin. Transl. Radiat. Oncol. 34 (2022) 51–56.

[46] P. Li, C.R. Du, W.C. Xu, Z.L. Shi, Q. Zhang, Z.B. Li, S. Fu, Correlation of dynamic changes in gamma-H2AX expression in peripheral blood lymphocytes from head and neck cancer patients with radiation-induced oral mucositis, Radiat. Oncol. 8 (2013) 155.

[47] H.V. Goutham, K.D. Mumbrekar, B.M. Vadhiraja, D.J. Fernandes, K. Sharan, G. Kanive Parashiva, S. Kapaettu, S.R. Bola Sadashiva, DNA double-strand break analysis by gamma-H2AX foci: a useful method for determining the overreactors to radiation-induced acute reactions among head-and-neck cancer patients, Int J Radiat Oncol Biol Phys 84 (5) (2012) e607–e612.

[48] A.M. Laheij, J.J. de Soet, P.A. von dem Borne, E.J. Kuijper, E.A. Kraneveld, C. van Loveren, J.E. Raber-Durlacher, Oral bacteria and yeasts in relationship to oral ulcerations in hematopoietic stem cell transplant recipients, Support. Care Cancer 20 (12) (2012) 3231–3240.

[49] S.-H. Ahn, S.-M. Chun, C. Park, J.-H. Lee, S.-W. Lee, T.-H. Lee, Transcriptome profiling analysis of senescent gingival fibroblasts in response to Fusobacterium nucleatum infection, PLoS One 12 (11) (2017) e0188755.

[50] P.G. Stathopoulou, M.R. Benakanakere, J.C. Galicia, D.F. Kinane, Epithelial cell pro-inflammatory cytokine response differs across dental plaque bacterial species, J. Clin. Periodontol. 37 (1) (2010) 24–29.
[51] S. Ji, J.E. Shin, Y.S. Kim, J.-E. Oh, B.-M. Min, Y. Choi, Toll-like receptor 2 and NALP2 mediate induction of human beta-defensins by Fusobacterium nucleatum in gingival epithelial cells, Infect. Immunity 77 (3) (2009) 1044–1052.
[52] T.V. Phan, Y. Oo, T. Rodboon, T.T. Nguyen, L. Sariya, R. Chaisuparat, W. Phoolcharoen, S. Yodmuang, J.N. Ferreira, Plant molecular farming-derived epidermal growth factor revolutionizes hydrogels for improving glandular epithelial organoid biofabrication, SLAS Technol. (2023).
[53] C.L. Tu, A. Celli, T. Mauro, W. Chang, Calcium-sensing receptor regulates epidermal intracellular Ca(2+) signaling and re-epithelialization after wounding, J. Invest. Dermatol. 139 (4) (2019) 919–929.
[54] Y. Liu, X. Yang, Y. Liu, T. Jiang, S. Ren, J. Chen, H. Xiong, M. Yuan, W. Li, H.G. Machens, Z. Chen, NRF2 signalling pathway: new insights and progress in the field of wound healing, J. Cell. Mol. Med. 25 (13) (2021) 5857–5868.
[55] H. Takano, Y. Momota, K. Kani, K. Aota, Y. Yamamura, T. Yamanoi, M. Azuma, gamma-Tocotrienol prevents 5-FU-induced reactive oxygen species production in human oral keratinocytes through the stabilization of 5-FU-induced activation of Nrf2, Int. J. Oncol. 46 (4) (2015) 1453–1460.
[56] X.X. Yan, H.L. Li, Y.T. Zhang, S.Y. Wu, H.L. Lu, X.L. Yu, F.G. Meng, J.H. Sun, L.K. Gong, A new recombinant MS-superoxide dismutase alleviates 5-fluorouracil-induced intestinal mucositis in mice, Acta Pharmacol. Sin. 41 (3) (2020) 348–357.
[57] M.M. Grant, A.E. Scott, J.B. Matthews, H.R. Griffiths, I.L.C. Chapple, Pre-conditioning of gingival epithelial cells with sub-apoptotic concentrations of curcumin prevents pro-inflammatory cytokine release, J. Periodontal. Res. 58 (3) (2023) 634–645.
[58] S. Kurinna, K. Seltmann, A.L. Bachmann, A. Schwendimann, L. Thiagarajan, P. Hennig, H.D. Beer, M.R. Mollo, C. Missero, S. Werner, Interaction of the NRF2 and p63 transcription factors promotes keratinocyte proliferation in the epidermis, Nucl. Acids Res. 49 (7) (2021) 3748–3763.
[59] K. Talaei, S.A. Garan, B.M. Quintela, M.S. Olufsen, J. Cho, J.R. Jahansooz, P.K. Bhullar, E.K. Suen, W.J. Piszker, N.R.B. Martins, M.A. Moreira de Paula, R.W. Dos Santos, M. Lobosco, A mathematical model of the dynamics of cytokine expression and human immune cell activation in response to the pathogen staphylococcus aureus, Front. Cell. Infect. Microbiol. 11 (2021) 711153.
[60] E. Aihara, C.L. Hentz, A.M. Korman, N.P.J. Perry, V. Prasad, G.E. Shull, M.H. Montrose, In vivo epithelial wound repair requires mobilization of endogenous intracellular and extracellular calcium, J. Biol. Chem. 288 (47) (2013) 33585–33597.
[61] C. Justet, J.A. Hernandez, A. Torriglia, S. Chifflet, Fast calcium wave inhibits excessive apoptosis during epithelial wound healing, Cell Tissue Res. 365 (2) (2016) 343–356.
[62] Y.H. Liao, K.H. Chiang, J.M. Shieh, C.R. Huang, C.J. Shen, W.C. Huang, B.K. Chen, Epidermal growth factor-induced ANGPTL4 enhances anoikis resistance and tumour metastasis in head and neck squamous cell carcinoma, Oncogene 36 (16) (2017) 2228–2242.
[63] A. Blakaj, M. Bonomi, M.E. Gamez, D.M. Blakaj, Oral mucositis in head and neck cancer: evidence-based management and review of clinical trial data, Oral Oncol. 95 (2019) 29–34.
[64] A. Villa, S.T. Sonis, Radiotherapy-induced severe oral mucositis: pharmacotherapies in recent and current clinical trials, Expert Opin. Investig. Drugs 32 (4) (2023) 301–310.
[65] X. Qu, X. Guo, T. Zhu, Z. Zhang, W. Wang, Y. Hao, Microneedle patches containing mesoporous polydopamine nanoparticles loaded with triamcinolone acetonide for the treatment of oral mucositis, Front. Bioeng. Biotechnol. 11 (2023) 1203709.
[66] S. Saghazadeh, C. Rinoldi, M. Schot, S.S. Kashaf, F. Sharifi, E. Jalilian, K. Nuutila, G. Giatsidis, P. Mostafalu, H. Derakhshandeh, K. Yue, W. Swieszkowski, A. Memic, A. Tamayol, A. Khademhosseini, Drug delivery systems and materials for wound healing applications, Adv. Drug Deliv. Rev. 127 (2018) 138–166.
[67] R. Tzach-Nahman, R. Nashef, O. Fleissig, A. Palmon, L. Shapira, A. Wilensky, G. Nussbaum, Oral fibroblasts modulate the macrophage response to bacterial challenge, Sci. Rep. 7 (1) (2017) 11516.
[68] C. Chen, Q. Zhang, W. Yu, B. Chang, A.D. Le, Oral mucositis: an update on innate immunity and new interventional targets, J. Dent. Res. 99 (10) (2020) 1122–1130.
[69] G. Muniraj, R.H.S. Tan, Y. Dai, R. Wu, M. Alberti, G. Sriram, Microphysiological modeling of gingival tissues and host-material interactions using gingiva-on-chip, Adv. Healthc. Mater. 12 (32) (2023) e2301472.
[70] A.M. Laheij, J.E. Raber-Durlacher, R.G. Koppelmans, M.-C.D. Huysmans, C. Potting, S.J. van Leeuwen, M.D. Hazenberg, M.T. Brennan, I. von Bültzingslöwen, J.-E. Johansson, Microbial changes in relation to oral mucositis in autologous hematopoietic stem cell transplantation recipients, Sci. Rep. 9 (1) (2019) 1–11.
[71] J.S. Bruno, G.H. Al-Qadami, A. Laheij, P. Bossi, E.R. Fregnani, H.R. Wardill, From pathogenesis to intervention: the importance of the microbiome in oral mucositis, Int. J. Mol. Sci. 24 (9) (2023).